The Australian National University

A Control System For Achieving Rapid Controlled Motions From Shape Memory Alloy (SMA) Actuator Wires

Yee Harn Teh
4011704

Supervisor: Dr. Roy Featherstone

A Thesis submitted in part fulfilment of the degree of Bachelor of Engineering at the Australian National University

June 2003

Acknowledgements

There are many who have made contributions, both directly and indirectly to the completion of this thesis. I would like to name a few.

First of all, I would like to sincerely thank my supervisor, Dr. Roy Featherstone, whose help has been enormous and whose enthusiasm has sparked my own in this wonderful work. His ideas and suggestions had frequently created jigsaw puzzles with many of the pieces missing throughout the entire project, which had made learning a very steep and difficult process for me. Yet they made all the efforts and time spent worthwhile.

I would like to express my gratitude to my parents and family, who have made me the person that I am now and who have given me the opportunity to thread my own path in life, but have never left me without support and love.

The staffs of the Research School of Information Sciences and Engineering (RSISE) at ANU had been extremely helpful, especially Jason Chen and Luke Cole whose mechanical and electrical expertise have helped construct the experiment rig and made this project possible. I would also like to acknowledge that this project was undertaken as a Summer Research Project at RSISE during the summer of 2002/03 with significant support and assistance from the Research School.

Finally, I would like to thank Aya, Ray and Xiao Wuan who were helpful enough to read my draft thesis, and provide such valuable feedback.

Claims of Originality

This thesis contains no material that has been accepted for the award of any other degree or diploma in any University. To the best of my knowledge, this thesis contains no material previously published, or results or any work by any other person, except where due reference is made in text.

Yee Harn Teh
June 2003

Abstract

Shape Memory Alloys (SMAs) are a group of metallic materials that demonstrate the ability to return to some previously defined shape via a phase transformation induced by thermal procedure. Basically, wires made from these alloys can be plastically deformed at some relatively low temperature, and upon heating will return to their shape prior to the deformation. A specially manufactured alloy of nickel and titanium (NiTi), called Flexinol^{tm}, is one of many that can generate significant force upon changing shape and is of commercial interest.

A lot of research and commercial work have been conducted on SMAs but only a few truly investigated the application of SMAs in an aggressive and robust control environment. In this thesis, control systems using the concept of relay control are applied to the system of a pair of SMA Flexinol^{tm} wires in antagonistic orientation. The objective is to achieve fast coordinated motion control of the robotic device.

The experimental set-up and the experiment rig that houses the SMA actuators are custom designed and constructed at the Research School of Information Sciences and Engineering at ANU. Properties of these Flexinol^{tm} wires were examined and experiments were carried out to develop an improved version of the two-level relay controller designed by Danny Grant for his PhD thesis in 1999. This control system utilises a power limiter mechanism that controls extremely high power inputs to the actuators for increased speed. Both Grant's controller and the improved control system were applied to the experimental set-up of SMA actuator wires and results were analysed to compare the performances of both controllers.

The experimental results had shown that substantially faster responses of the system had been achieved using the improved control system compared to the two-level relay controller. However, the problem of limit cycle at the steady state needs to be overcome with further improvements in both the control system and the experiment rig.

This project has made rapid motion control of SMA actuators wires possible. Potential development and improvements for faster and more accurate SMA wire actuation are extremely possible with the experimental set-up.

Table of Contents

List of Figures

List of Tables

Chapter 1: Introduction

In this chapter, we will begin with a short introduction to Shape Memory Alloys (SMAs) and their applications. The motivation and the research objectives of this thesis will be covered in Section 1.2 and followed by a review of the literature in Section 1.3. Finally, a quick outline of the overall thesis will be covered at the end of this chapter.

1.1 Shape Memory Alloys

Many systems, including manufacturing, automobiles, plants and machines depend on actuators as the driving mechanism. These actuators use electric, hydraulic or pneumatic technologies. As applications become more diverse and compact, new ways or types of actuators are needed to make these ideas work. These new technologies open the way to novel actuators such as Shape Memory Alloys, piezoelectrics and nanomachines.

Shape Memory Alloys (SMAs) are one of the exciting new technologies that offer many advantages and usages. Some of their wonderful properties are their high force-to-weight ratio, incredibly small size and volume, as well as their low cost compared to conventional actuators. However, SMAs are not free from drawbacks such as the non-linearities and hysteresis that are present in the phase transitions, their limited strain and bandwidth. The potentials of SMAs and their feasibility in robotic or other commercial applications are still being explored. According to Hodgson and Wu [**5**], it is anticipated that many engineering domains in the near future will have use of SMAs.

One of the most common shape memory alloys is the alloy of nickel-titanium (NiTi). Advantages of NiTi compared to other SMAs are its greater shape memory strain, thermal stability, higher ductility and excellent corrosion resistance [**5**]. Wires of Flexinol^{tm}, which is a trade name for NiTi actuator wires specifically manufactured by Dynalloy Inc., are processed to contract like muscles when electrically heated and can easily be stretched as they cool back to ambient temperature.

This work uses Flexinol^{tm} wires with a diameter of 100 microns (0.004 inch) as actuators in a custom-designed experimental and control set-up. A more detailed background of SMAs as well as the experimental set-up for this work will be covered in Chapter 2.

1.2 Motivation and Research Objectives

Traditional forms of actuators such as motors necessitate the use of large and heavy supporting apparatus and are usually very noisy. Shape Memory Alloys have the advantage of more compact and silent actuation. However, at the current stage of research and development, SMAs are yet to be able to replace conventional actuators for most applications. Due to their hysteretic nature and non-linearities, SMAs remain a slow and inefficient type of actuation compared to a motor. They remain mostly as experimental robotic devices.

However, works by researchers and leaders in the field are slowly changing this view. Work by Grant in 1999 [**6**] is an example that SMA actuators are capable of fast and accurate motion. Using relay controller and an antagonistic set-up, Grant demonstrated that significant improvements had been made in terms of speed and accuracy of control.

This project builds on the works of Grant and his relay controller on SMA antagonistic wire pairs. The primary objective of this work is to implement a control system to further increase the speed and aggressiveness of actuation. This is done by implementing Grant's relay controller with an additional power limiter mechanism.

Grant's controller used only safe current inputs for Flexinol^{tm} wire actuation but the power limiter mechanism allows dangerously higher currents into the system. It is also our goal to compare results and performance of Grant's relay controller with the controller with power limiter mechanism.

1.3 Literature Survey

This section presents a brief literature overview of Shape Memory Alloys. In particular, a brief history of SMAs and previous work on SMA modelling, actuation and control will be presented.

1.3.1 Brief History of Shape Memory Alloys.

Many different metal alloys had been discovered to display shape memory properties. In fact, the first recorded observation of the shape memory effect was made by Chang and Read in 1932 (Chang and Read, 1951, cited in [**5**]). The current most commonly used is a near-binary mixture of nickel and titanium, called Nitinol (*Ni-Ti-NOL*) since it was first developed at the US Naval Ordinance Laboratory in 1961 (Buehler, Gilfrich and Wiley, 1963, cited in [**7**] Gorbet 1996).

Within 10 years, a number of commercial products that implemented the shape memory effect were available. Most of these products usually involved simple components with the property of one-time shape memory change. Nowadays, applications of SMAs include force actuators, proportional control, superelastic applications, medical industry applications, micro-robotics and many other usages [**5**] but none is used in high-speed applications.

More shape memory alloys were discovered and investigated as the shape memory effect and their properties became better understood. This paved the way for extensive research in modelling SMAs for robotic actuations.

1.3.2 SMA Modelling.

In control system design, a model is invaluable as a design aid. One of the hot topics of SMA research is the modelling of their hysteretic nature. It is the presence of this wide hysteresis loop in the phase transformation of SMAs that makes accurate modelling of SMA actuators difficult. Basically, models that have been proposed so far can be divided into two categories: linear and non-linear.

In Baz, Imam and McCoy 1990 cited in [**7**], a simple model assuming only one transformation temperature was developed. This model assumes that all phase transformations, from martensite to austenite, and vice versa, occurs at this temperature. The contraction of the SMA wire is calculated using a piece-wire function of temperature. Other examples of linear models are made by Kuribayashi and Hashimoto, cited in Gorbet 1999 [**7**].

Linear models are usually 'over-simplification of the actual thermal dynamics of the alloy', according to Gorbet. Some researchers such as Ikuta, Lin and Madill proposed non-linear models which try to explain and model the hysteresis present in the phase change of SMAs.

1.3.3 SMA Actuation and Control.

The usage of SMAs in robotic applications has become increasingly significant. Most of these SMA actuators are used either in the form of long straight fibres or as coils.

However, despite extensive research into SMA actuation and control, only a few ever researched into accurate but aggressive motion of SMA actuators such as [**6**] and [**12**]. Grant had shown that SMAs are capable of fast and accurate actuation using relay control with an antagonistic actuator arrangement. His results indicated that SMAs can be used in a broad class of applications such as force control, position control and vibration isolation. Rediniotis and Lagoudas [**12**] had shown that excellent tracking at actuation bandwidths of 20 Hz could be achieved for SMA wire contraction.

Yet, research on the aggressiveness and robustness of SMA motion control is considered little compared to other research topics in SMAs. This project represents another opportunity to investigate the performance of SMA wire actuators in high-speed control.

1.4 Challenges

Developing a control system that can achieve rapid controlled motion of SMA actuator wires poses several design challenges:

- A complete experimental set-up has to be constructed and tested to ensure proper functionality
- Experimental set-up must provide accurate and useful feedback data regarding the state of the actuators and their position.
- Experiment rig must have potential for hardware improvements and development
- Shape Memory Alloy actuation has non-linear properties and hysteretic nature
- The range of actuation must be large enough for visible and useful motion of the robotic device

To achieve the underlying objectives of this project, the successful design and construction of a complete experimental set-up that incorporates both hardware and software components must be carried out. This long-term process will be reflected in the thesis.

1.5 Thesis Outline

This thesis is divided into 6 chapters.

Chapter 2 begins with some background information on SMAs such as their phases, phase transitions, properties and limitations. This chapter will also include a description of the experimental set-up used in the project.

Chapter 3 first deals with the testing of the hardware and software components to ensure the set-up can perform to meet our objectives. Before a control system could be implemented to control the actuators, the experimental set-up needs to be tested and software modules that deal with data acquisition and encoder initialisation need to be designed. Procedures for the testing experiments will be briefly described. Next, modelling experiments are examined in order to develop an improved control system. Results obtained will be applied in the design of the power limiter mechanism with the two-level relay controller.

Chapters 4 and 5 present the two control systems that have been implemented in the project. The first is the two-level relay controller adapted from Grant [**6**] and the second is the improved relay controller with an additional power limiter mechanism. Chapter 4 will begin with some general design issues of a control system. Grant's two-level relay controller will be examined and results of the control system will be presented.

Chapter 5 details the design of the power limiter mechanism and its implementation in an improved control system will be presented. The chapter ends with a comparison of results between the two different control systems.

Finally, this thesis concludes with Chapter 6 with some future research and improvement issues. It is hoped that this document will be an aid to students working in aggressive control of Shape Memory Alloy actuators.

Chapter 2: Background and Experimental Set-Up

This chapter begins with some background information on Shape Memory Alloys and their properties in general. A description of their phases and the phase transformation, the limitations of SMAs as well as some important properties of Flexinol^{tm} will be presented. Section 2.2 deals with the experimental set-up and includes a description of the experiment rig, the pantograph device as well as other equipments and components used in this work.

2.1 Properties of Shape Memory Alloys

This section describes the basic theory required to understand the workings of Shape Memory Alloys. Much of the explanation had been drawn from [**5**], [**6**] and [**7**]. For more in-depth understanding of SMAs, the reader is encouraged to consult these sources.

2.1.1 The Shape Memory Effect.

Shape Memory Alloys are a group of metallic materials that is distinguished by their ability to return to a specific shape or size prior to deformation through a temperature dependent phase change

When a Shape Memory Alloy is in its martensitic structure, it can be easily deformed to a new shape. However, when it is heated through a suitable range of temperatures, it changes to its austenite phase and recovers its previous shape. This phase transformation process is known as the shape memory effect and forms the basis of research in SMA actuation.

2.1.2 Phases of SMA.

In terms of practical applications, a NiTi SMA can exist in three different crystal structures or phases called martensite, stress-induced martensite and austenite as noted by [**10**] Mihalcz 2001. At low temperature, the alloy exists as martensite. It is weak, soft and more deformable. Stressed-induced martensite or superelastic NiTi is highly elastic (rubber-like) and is present at a temperature that is slightly above its transformation temperatures. The austenite is the stronger, higher temperature phase present in NiTi. For the purpose of this work, we will concentrate on two phases – the martensite and austenite phases.

The phase transformation from martensite to austenite and back again, are described by a wide hysteresis loop, shown in Fig 2.1 (adapted from [**5**]). The phase transitions are characterised by four transformation temperatures: (i) A_s, the austenite start temperature; (ii) A_f, the austenite finish temperature; (iii) M_s, the martensite start temperature; and (iv) M_f, the martensite finish temperature.

To the left of the martensite finish temperature M_f, only martensite is present. To the right of the austenite finish temperature A_f, only austenite is present. In between M_f and A_f, there is a combination of martensite and austenite. The hysteresis, ΔT, is defined as the temperature difference

between a phase transformation upon heating and cooling. This transformation hysteresis varies according to the alloy system.

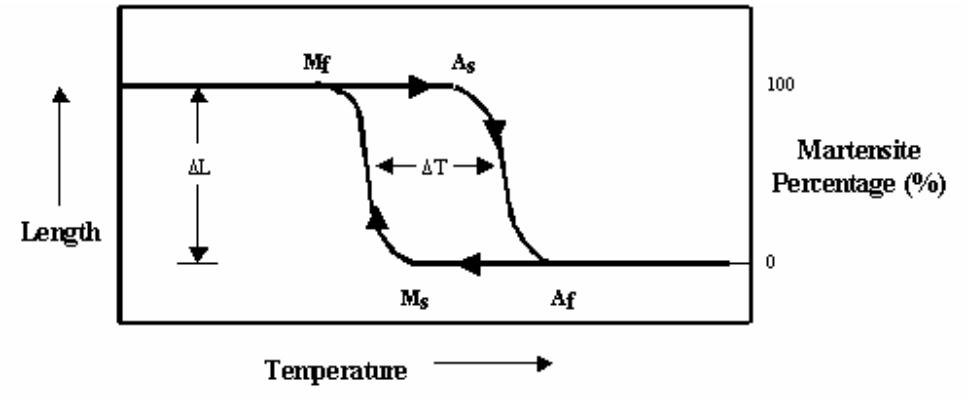

Figure 2.1 Hysteresis Curve and Transformation Temperatures of SMA.

The two phases of NiTi and their transformations are depicted by the 2-dimensional matchbox model in Figure 2.2 (adapted from [7]). The stronger austenite phase, also known as the parent phase, has a cubic atomic structure and is represented by squares in Fig 2.2. As the alloy cools to the martensite phase in a process called twinning, the crystal structure becomes rhomboidal and is represented by collapsed matchboxes. When heated again, it returns to its original cubic form in the parent phase.

When the SMA in martensite phase is subjected to external force, deformation causes its structure to become detwinned. As it is reheated past A_s, the austenite start temperature, the detwinned martensite begins to form into austenite. When the temperature exceeds A_f eventually, the alloy will have reverted to full austenite phase and contracted back to its original length.

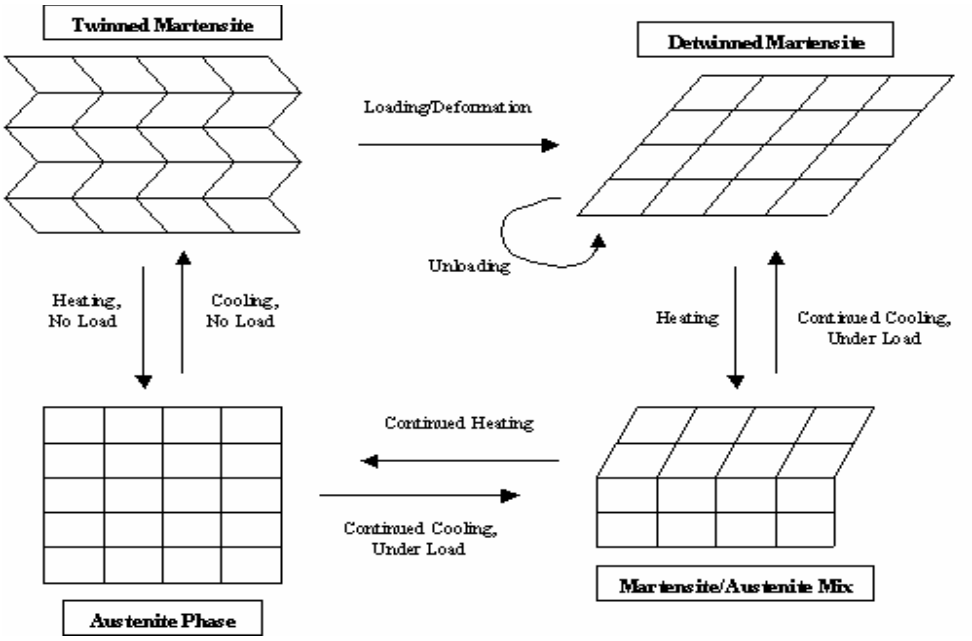

Figure 2.2 Two-Dimensional Crystal Structures and Phase Transformations of SMA.

The deformed martensite will not recover loading strain upon unloading of the force directly. In order for strain recovery to occur, the material must be heated for the phase transformation process from martensite to austenite. Therefore, the martensite structure is not elastic, but thermo-elastic or heat-recoverable [**7**].

Figure 2.3 (adapted from [**6**]) depicts the stress-strain curves of both martensite and austenite of SMAs. When an external stress is applied to the alloy when it is fully martensitic, the alloy deforms elastically (curve 1 in Fig. 2.3 (a)). If the stress exceeds the martensite yield strength, detwinning occurs and a large non-elastic deformation will result until the structure is fully detwinned (curve 2 in Fig. 2.3 (a)). The martensite is strain recoverable up to this stage. However, further increase in stress causes the detwinned structure to deform (curve 3 in Fig. 2.3 (a)) until the external stress begins to break the atomic bonds between the martensite layers, resulting in permanent plastic deformation (curve 4 in Fig. 2.3 (a)). The strain at which this permanent deformation occurs in NiTi material is 8% according to the published properties by SMA Inc. [**14**]. Most application will restrict strains between 4-6 % or lower.

For the austenite phase however, it has a higher yield strength compared to martensite. Initially, the alloy will behave elastically (curve 1 in Fig 2.3 (b)) until the stress exceeds its yield strength. From that point onwards, plastic deformation will ensue causing unrecoverable stretching upon unloading (curves 2 and 3 in Fig 2.3 (b)).

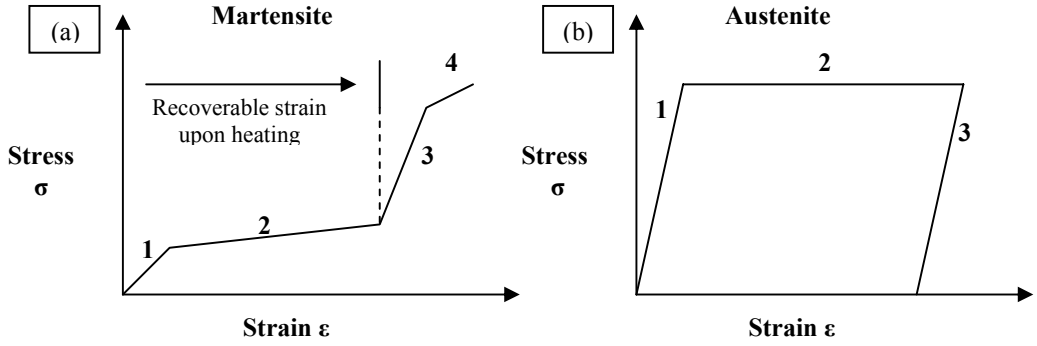

Figure 2.3 Stress-Strain Curves of (a) Martensite and (b) Austenite.

2.1.3 Properties during Transformation.

Most of the physical properties of austenite and martensite vary during phase transformations. Based on Harrison (1990), cited in [**5**], the properties that change during transformation include Young's Modulus, resistance, heat capacity, latent heat of transformation and thermal conductivity. Non-linearities exist in the possible range of these properties and are also dependent on alloy composition, processing and the number of activated cycles.

2.1.4 Advantages of SMA.

Other than the small sizes and high force densities compared to conventional actuators, SMAs have other advantages. First, SMA actuators can be used as 'Direct Drive Linear Actuators' as they can be directly actuated using electrical current requiring little or no gear reduction or motion amplification hardware according to Rediniotis and Lagoudas [**12**]. This feature allows the

miniaturisation of actuation system where conventional motors lack this ability to overcome space limitations. Secondly, SMAs produces silent actuation compared to the noise of actuators such as motors and gears. A third advantage of SMAs is the low driving voltages required when electrically powered. SMAs such as NiTi can be actuated with very low voltages, thus needing simple power supply hardwares.

2.1.5 Limitations of SMA.

However, SMA actuation is not free of drawbacks. One of the reasons for its current limitations in robotics is because SMAs are highly non-linear and many of their properties are phase-dependent. In addition, the wide hysteresis loop in its contraction and resistance makes it very difficult to control.

In terms of mechanical limitations, SMAs have a limited percent strain and a low bandwidth. The absolute strain is approximately 8 %, but the practical strain is only about 4-5 %. SMAs usually cannot achieve high motion bandwidth due to the inherent hysteresis and slow cooling rate. Other than that, actuation loss and fatigue over repetitive cycle loading remain as extensive research issues. Some of these limitations will be addressed further in Chapter 4.

2.1.6 Properties of NiTi and Flexinol^{tm}.

The following are some selected properties of NiTi taken from the datasheet of [**14**] which are more related to this work. The complete list of properties can be found in Appendix A.

Transformation Properties:

Transformation Temperature ……..…….. -200 to 110 deg. C

Transformation Strain

For a single cycle …… max 8 %

For 100 cycles ……. 6 %

For 100,000 cycles …….. 4 %

Hysteresis (for full martensite to austenite transition)…..……...… 30 to 50 deg. C

Electrical Properties:

Resistivity

Austenite ……..…….. Approx. 100 micro-ohms * cm

Martensite ……..……...… Approx. 80 micro-ohms * cm

*Approximate Safe Current for Wire with 0.004” diameter …….…..….. 180 mA

* The safe current is the current which takes one second to heat the wire and can be left on without overheating it

---

Table 2.1 Selected Properties of NiTi Related to This Work.

These NiTi properties also apply for Flexinol^{tm} wires as well[1].

[1] This information was obtained via private e-mail communication with Daniel Dorn, a project manager of Dynalloy Inc. on 23 April 2003.

2.2 Experimental Set-Up

A block diagram of the top-level experimental architecture is shown in Fig 2.4.

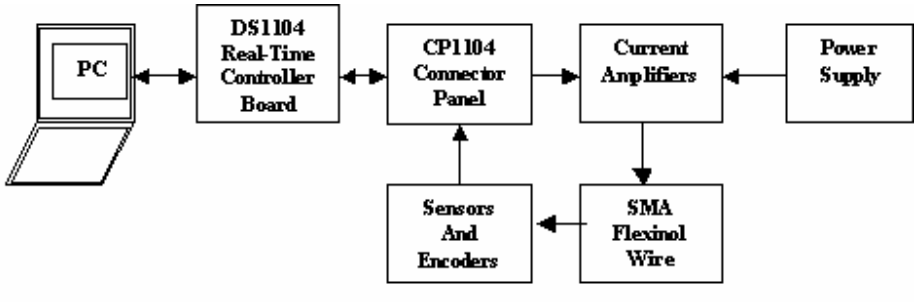

Figure 2.4 Overall Experimental Set-up and Its Main Components

Experiments in Chapter 3 and the control designs in Chapter 4 were implemented in the Controls Lab at RSISE as shown in Fig 2.5. MATLAB/Simulink Real-Time toolbox and the dSPACE software called ControlDesk Standard were used. The dSPACE hardware consists of the DS1104 R&D Controller Board and the CP1104 I/O Connector Panel.

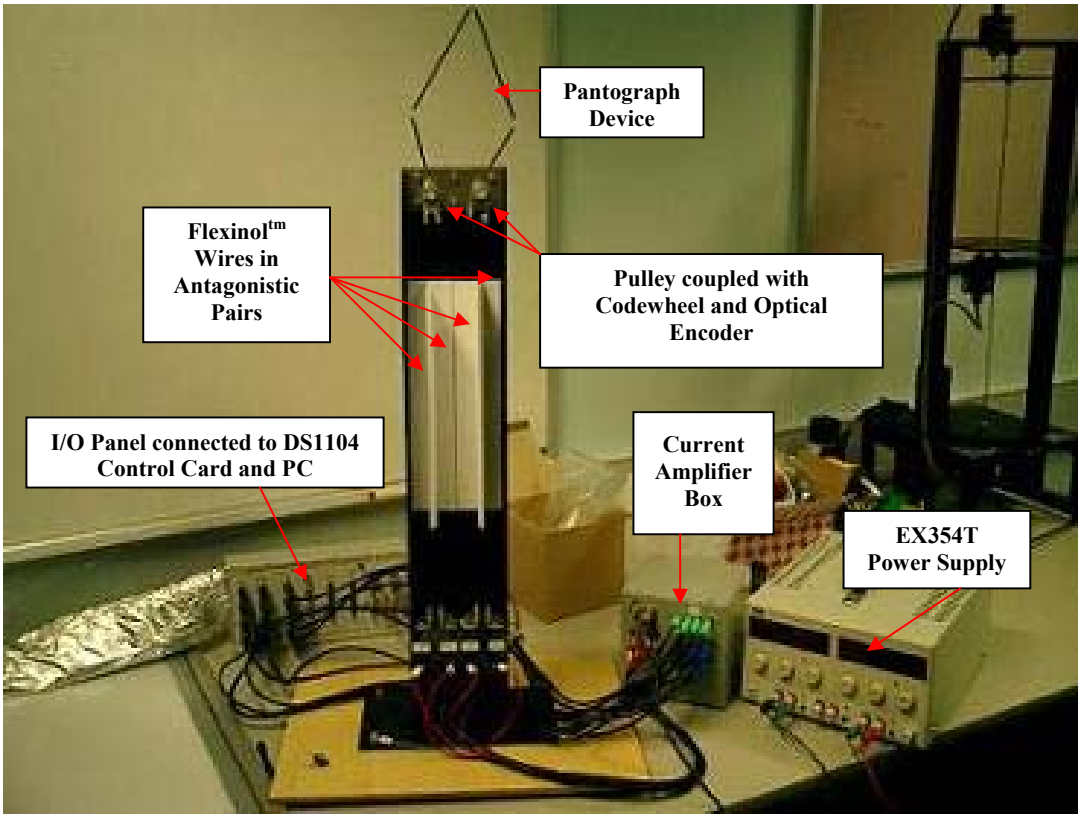

Figure 2.5 Experiment Rig and Other Components

The current amplifiers and experiment rig were custom designed by Dr. Roy Featherstone and constructed with the help of Dr. Jason Chen at RSISE. The Thurlby Thandar EX354T Bench Power Supplies provides high levels of power with a high-resolution controls setting. The SMA actuator

wires are housed in the experiment rig together with the optical encoders that measure the position and displacement of the actuators.

2.2.1 dSPACE.

The dSPACE software, ControlDesk, is a graphical user interface that provides the functions to control, monitor and automate experiments and make the development of controllers more efficient. The dSPACE hardware consists of the DS1104 R&D Controller Board and the CP1104 Connector Panel.

The Controller Board is a complete real-time control system based on a 603 PowerPC processor at 250 MHz. The Real-Time Interface (RTI) forms the interface between Simulink and the dSPACE hardware. It is used to build real-time code, and to download and execute this code on dSPACE hardware. Further details can be obtained from the dSPACE guides [**2**] and [**3**].

The following features of the Connector Panel are used in the project:

- Eight parallel Digital-to-Analog Converters (DAC) for digital outputs
- Four 12-bit parallel Analog-to-Digital Converters (ADC) for analog inputs
- One 16-bit ADC with four multiplexed analog inputs
- Two digital Incremental Encoder Interface for the optical encoders

2.2.2 Experiment Rig.

The experiment rig shown in Figure 2.6 can house up to four Flexinol^{tm} wire actuators, two HEDS encoder modules as well as a pantograph device. The actuators are arranged in antagonistic formations using pulleys. The pulleys are coupled with a codewheel that can be used to detect rotary position of the pulley with the encoder module. Each SMA wire is electrically connected to one of the four amplifiers in parallel (housed in the amplifier box shown in Fig 2.5). The optical encoder modules are directly connected to the I/O Connector Panel.

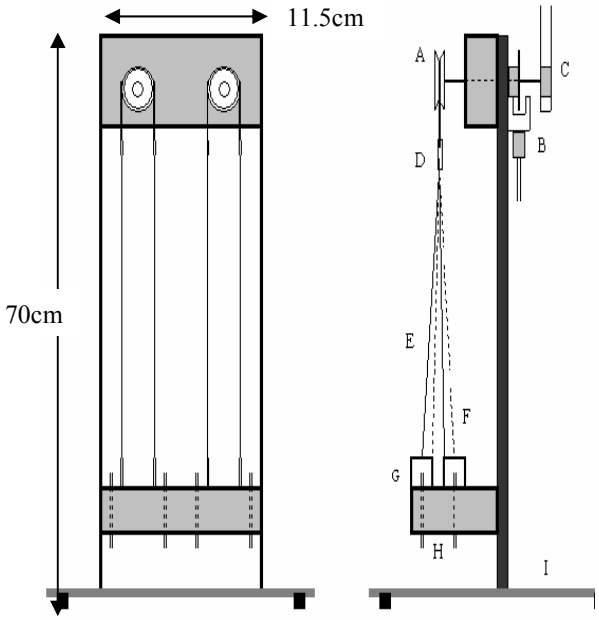

A. Pulley with 1.5cm diameter grove carrying inextensible chord
B. HEDS Optical Encoder Module with 2" encoder disk
C. Optional load (eg. copper rod or pantograph device)
D. Aluminium bracket with SMA wire and inextensible chord looping through
E. SMA actuator wire
F. Optional extra SMA wire for more force
G. Metal brackets acting as mechanical anchors and electrical contacts for SMA wire
H. Electrical contacts with SMA wire from amplifier circuit
I. Experiment rig attached to wooden stand for stability

Note: Height of rig is approximately 70 cm
Width is approximately 11.5 cm

Figure 2.6 Front and Side Views of Experiment Rig (Not To Scale)

2.2.3 Flexinol^{tm} Wires and The Antagonistic Set-Up.

The diameter of the Flexinol^{tm} actuator wires used is approximately 100 microns (0.004 inch). They are set-up in an antagonistic pair arrangement in the experiment rig. The reason is, the shape memory effect is usually one-way. This means that upon cooling, the SMA wire does not undergo any shape change and with a non-antagonistic setting, it cannot be actuated in the opposite direction. Hence, it is necessary to provide a biasing force or to actuate it in the opposite direction and this can be done using weights, springs or the antagonistic set-up [**6**]. Another reason is to reduce the effects of the wide hysteresis loop in the input-output relations of SMAs. This is implemented with the use of relay control. Further discussions will be given in Chapters 3 and 4.

2.2.4 Amplifier Circuits.

The main purpose of the amplifier circuit is to drive the SMA actuators. Actuation of SMA wires is based on the shape memory effect. This process is dependent on temperature. This is accomplished by applying a voltage drop across the wire causing current flow through the wire. The result is joule heating and thus actuation. To control the amount of current through the wire, the amplifier circuit shown in Fig 2.7 is constructed. It is a voltage-controlled (DAC Voltage) current-output (Current through SMA) circuit.

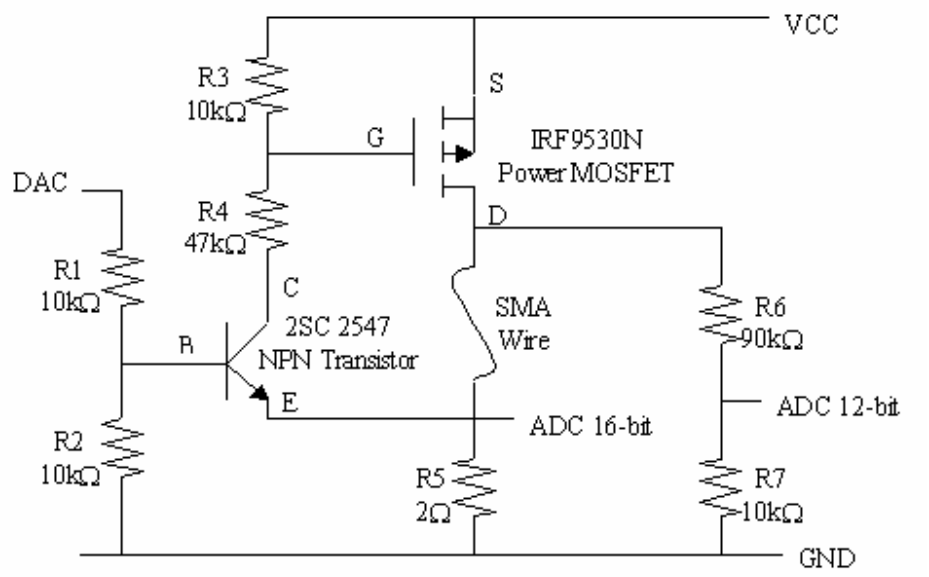

Figure 2.7 Amplifier Circuit To Drive One SMA Actuator Wire

The amplifier circuits are also specifically designed to allow the user to measure voltage values at two points as shown in the diagram using the ADCs of the Connector Panel. This allows the user to measure the input power and resistance of the SMA actuators as shown in Appendix B.4 for modelling and control design purposes.

As the experiment rig can house up to four wire actuators, we require four drive circuits in parallel, all on a single board. The amplifier box in Fig 2.5 houses the circuits.

2.2.5 HEDS Optical Encoder Module.

The HEDS optical encoder modules are manufactured and purchased from US Digital. A 2-inch encoder disk is coupled to each pulley actuated by the antagonistic SMA wire pairs on the experiment rig as presented in Fig 2.8.

The main purpose of the encoder module is to detect rotary position and displacement of the encoder disk when actuated by the wires. This is done using a lensed LED source and a monolithic detector IC to detect rotary movements of tracks on the encoder disk. The encoder modules are linked to the Incremental Encoder Interfaces on the Connector Panel. Further information regarding the HEDS module can be obtained from [**16**].

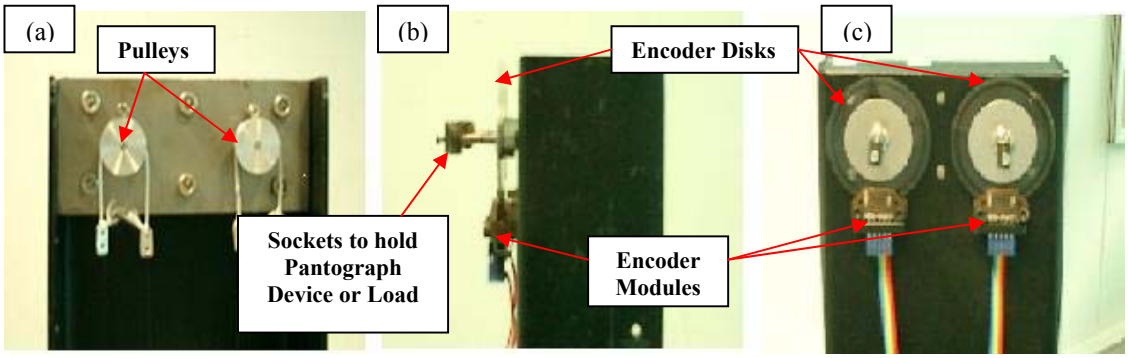

Figure 2.8 Views of the Encoder Modules and Pulleys. (a) Back View. (b) Side View. (c) Front View.

The encoder disk contains three channels or tracks as shown in Fig 2.9, two of which contains repeating sequence given in encoder lines 90° out-of-phase. The 2-inch disk used for this work has a resolution of 2048 CPR (Cycles Per Revolution of the disk) shown in Fig 2.9. This allows the encoder module to detect and measure only relative rotation angle changes from any initial position. A third track containing only one Index Pulse, provides an initialised zero-position for determining absolute rotary displacements for the experiments and control systems to follow. Further details of how to initialise the encoder modules will be discussed in Appendix B.

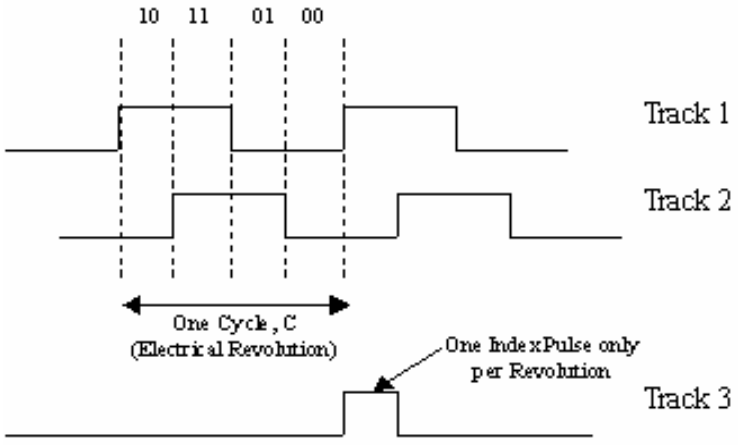

Figure 2.9 Channels/Tracks on Encoder Disk

2.2.6 Pantograph Device.

A pantograph is basically a drawing instrument. It is an optional application of the experiment rig. The device can be coupled to the two pulleys via the sockets in Fig 2.68. It can be actuated by two antagonistic pairs of the SMA actuators to act as a two degree-of-freedom planar robot. However, the control of the pantograph device is subjected to the time constraint of this project so further development should be made.

The pantograph device is constructed using carbon rods for lightness as well as hardness and connected using plastic hinges. Fig 2.10 shows a photo of the constructed pantograph.

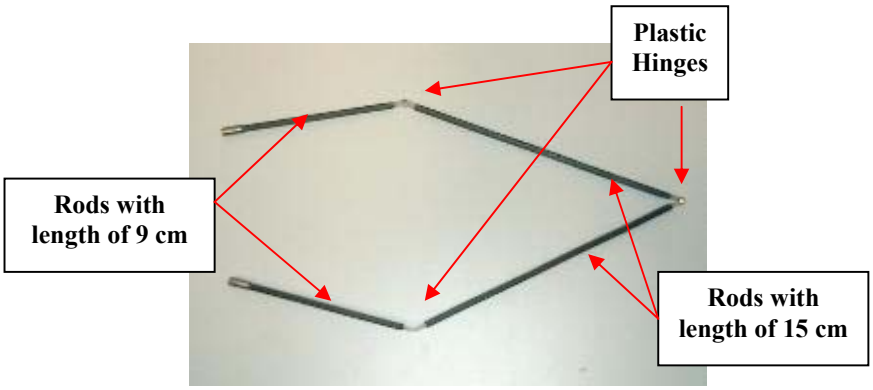

Figure 2.10 Pantograph Device

2.3 Chapter Summary

In this chapter, background knowledge on Shape Memory Alloys and their properties were presented. The experimental set-up and its crucial components used in this work were also briefly explained.

Chapter 3 will be concerned with testing and implementation using the experimental set-up described in this chapter. In particular, some of the hardware components need to be improved and modified. Software models such as the encoder initialisation module as well as the data acquisition and processing modules need to be designed before a control system can be applied to control the SMA wire actuation.

Chapter 3: Experimental Testing and Modelling

To ensure proper functioning, different aspects and components of the experimental set-up require designing and testing. Section 3.1 describes these. A Simulink model that aims to test the successful actuation of the Flexinol[tm] wires and the operation of all aspects of the set-up will follow in Section 3.2. Finally, in Section 3.3, modelling experiments will be examined and compared with theory. Results obtained will be applied in the design of the power limiter mechanism for our relay controller.

3.1 Experimental Set-Up and Design Issues

Before complete experiments and control systems could be run, every aspect and component of the experimental set-up, be it software or hardware, requires testing and designing. In this project, a lot of work had been done on developing and fabricating most components from scratch before a control system could work with the set-up.

Important hardware components of the experimental set-up include the experiment rig, the amplifier circuit box, the Flexinol[tm] actuators, the I/O Connector Panel and the wires that provided electrical connections between different components. Some of these components are custom designed and constructed at RSISE so they are prone to improper functioning or faulty connections. Other than that, software modules such as encoder initialisation and data processing also require design.

A summary of the various testing and designing procedures of the experimental set-up will be described in Tables 3.1 and 3.2. The motivations for these tasks as well as possible implications are also summarised. The reader should refer to Appendix B for detailed information on the experimental set-up procedures and design issues.

Simulink Module for Initialisation of HEDS Optical Encoder Module Motivation: ▪ Provide measurement of absolute rotation angle of the encoder disk with respect to a known initial position as well as the displacement of the actuator ▪ Simulink module designed can be used for positional data acquisition in control systems
Simulink Module for Analog Data Acquisition and Processing Motivation: ▪ Provide information on electrical properties of the SMA actuators during phase transformation such as resistance and input power values ▪ Simulink Module designed can be used in control systems Drawback: ▪ Significant noise in initial design requires filtering

Table 3.1 Software Design and Testing.

Standardisation of Flexinol^{tm} Wires Motivation: ▪ Ensure initial states and properties of each actuator wire are similar ▪ Ensure repeatability of procedure ▪ Replacement of wires can be made easily if a wire is damaged Drawback: ▪ Significant slack in the wires exists ▪ Reduced effective range of actuation
Safety Features of Experiment Rig Motivation: ▪ Isolation of actuator wires prevents short-circuiting and damage to actuators ▪ Experiment rig grounded to prevent electrocution due to dangerous current inputs
Safety Features of Amplifier Circuits Motivation: ▪ Testing of amplifier circuits and electrical connections prior to usage prevents damage to expensive actuators and field effect transistors ▪ Heat sinks installed to dissipate heat generated by high input power

Table 3.2 Hardware Design and Testing.

3.2 Testing of Overall Experimental Set-up

An experiment to test the working of the overall experimental set-up was designed (Refer to Fig C.3 in Appendix C for Simulink model of this experiment). The purpose is to ensure that different components can be integrated to function for the actuation of an SMA wire as well as the collection of useful data for further analysis.

One wire actuator was tested through open loop experiment using the experimental set-up described. Current is applied to the wire via the amplifier circuit using either a step or a ramp input DAC voltage from the dSPACE Board. A small weight of 10 grams is hung on the other side of the pulley to ensure the wire is taut. As we shall see in Section 3.2.1, responses of step input and ramp input will be examined. The issue of noisy analog data will be discussed in Section 3.2.2.

3.2.1 Results.

Each experimental run lasted approximately 30 seconds for step input and 60 seconds for ramp input during which the following data were recorded: DAC voltage, current through SMA, voltage across SMA, wire contraction and SMA resistance.

The responses of both step input and ramp input are presented in Fig 3.1 and Fig 3.2. These plots show some important features about the properties and performance of the SMA wire:

- A delay was observed as contraction initiated as it takes a finite amount of time for the Flexinol^{tm} wire to reach the austenite start temperature and commence contraction
- An almost linear, first order system rise to a maximum contraction was observed in both step and ramp responses. It was noted that the slope of the response was dependent on the magnitude of the input. The instantaneous step input resulted in a faster response compared to the ramp input.
- A reasonably stable steady state contraction was observed.
- A decay towards the initial configuration was observed when the step input ended and when the

ramp input decreased but it never reached its initial position. The small weight did not provide enough restoration force to fully stretch the wire as it transformed from austenite back to martensite.

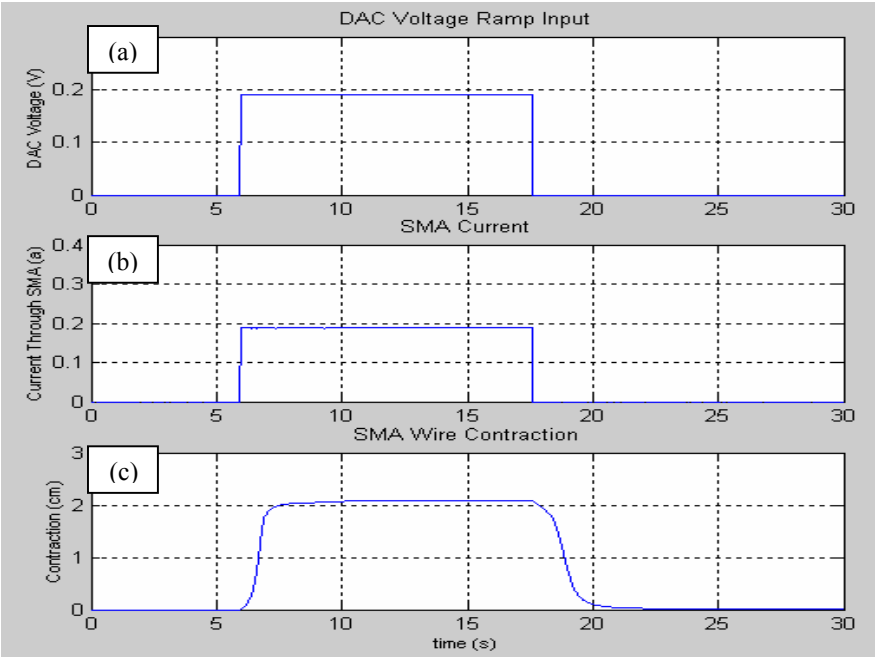

Figure 3.1 *Open Loop Step Response. (a) DAC Input Voltage. (b) Current through SMA. (c) SMA Wire Contraction.*

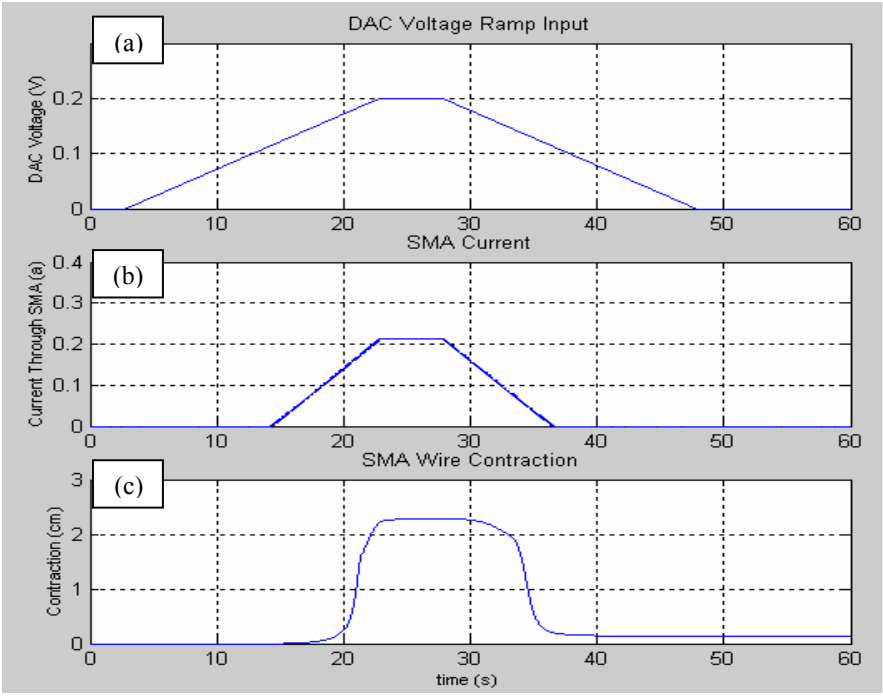

Figure 3.2 *Open Loop Ramp Response. (a) DAC Voltage. (b) Current through SMA. (c) SMA Wire Contraction.*

Although not shown in the graphs, it was noted that the slope of the response changed with the magnitude of the step input. Larger magnitudes resulted in faster responses. It was also observed that a saturation phenomenon occured in the contraction of the Flexinol[tm] wire for larger inputs. This is a result of the physical property of the wire as its typical strain is limited to 4%. These observations were also consistent with the results obtained by Mosley, Mavroidis and Pfeiffer in [**11**].

Fig 3.3 presents the observation of the hysteresis loop during the thermal cycle as the Flexinol[tm] wire was heated and then cooled. It is easily observed that the hysteresis profile of Fig 3.3 (a) agrees with the theoretical background of Shape Memory Alloys in Chapter 2. As current flows through the material, the temperature increases via joule heating. At the transformation temperature, the wire begins to contract at a faster speed until it is fully austenite, thus reaching a maximum contraction. As the wire is cooled under a load, the wire stretches back to its initial length.

Fig 3.3 (b) indicates the profile of the electrical resistance of the SMA wire during phase transformation. The slope of the graph (voltage over current) gives the electrical resistance value of the wire. One sees a change in the electrical resistance of the SMA wire as the material changes phase from martensite to austenite, and vice versa. It was noted in Fig 3.3 (a) and (b), that the wire is already fully austenite at approximately 0.18 A, which corresponds to the safe current level. Further increasing the current will only increase the temperature of the wire but will have no effect on the contraction of the wire.

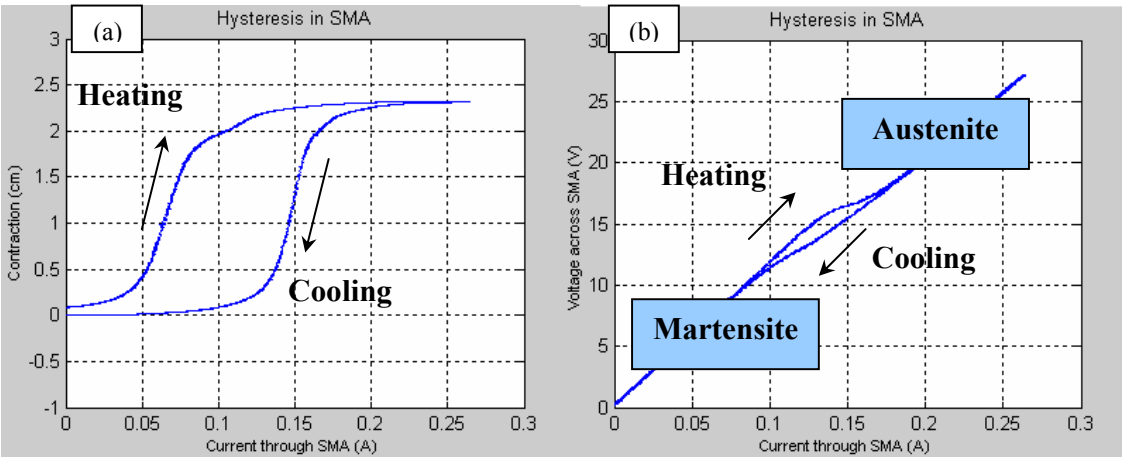

Figure 3.3 Observation of Hysteresis in SMA Wire during Ramp Input. (a) Contraction vs. SMA Current. (b) Voltage across SMA vs. SMA Current.

3.2.2 Noise Problem.

As can be seen from the results in Fig 3.4, there is significant amount of noise in our ADC analog data. A closer observation of the results indicates that the noise present is high-frequency noise. It was concluded that the amplifier circuit is picking up high-frequency signals from AM or FM radio waves. The RMS (root-mean-square) level of the noise was potentially too significant to be neglected and it would drastically affect the accuracy of our results.

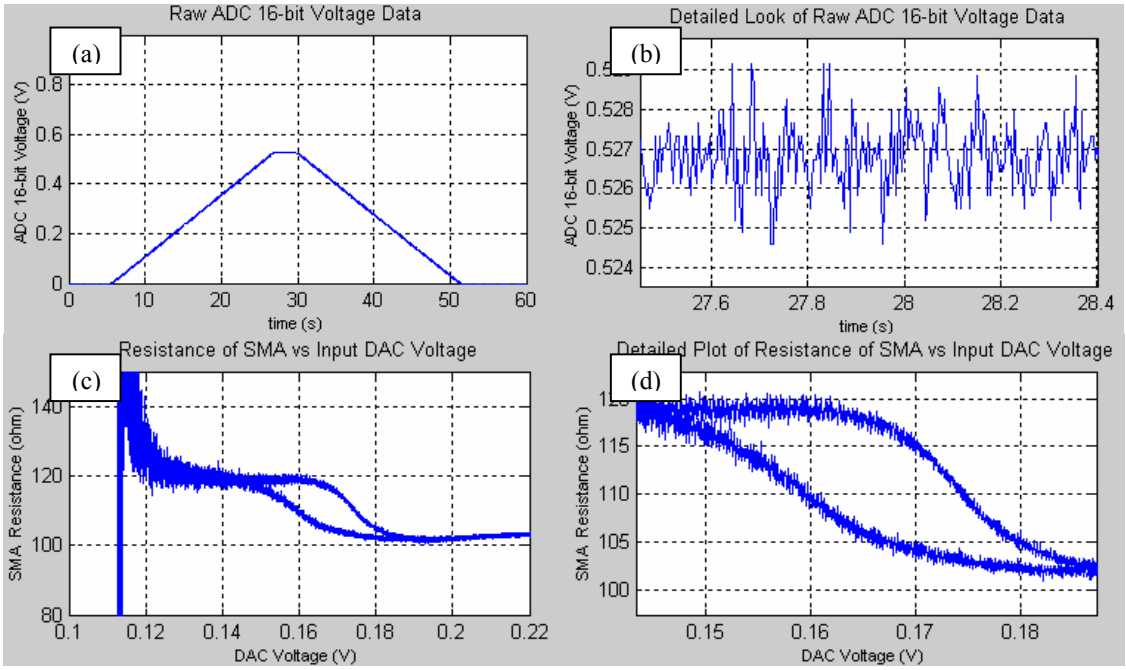

Figure 3.4 Analog Input Data with Noise. (a) Raw ADC 16-Bit Voltage. (b) Detailed Plot of (a) showing High Frequency Noise. (c) Plot of SMA Resistance vs DAC Voltage. (d) Detailed Plot of (c) showing the Effect of Noise on the Result.

Investigation was conducted to identify the origin of the noise. Modifications were made on the amplifier box and the cables between the PC and the CP1104 Connector Panel shielded. Temporary low-pass filters (LPFs) were implemented in the circuit with the intention of filtering out the high-frequency noise component but the problem persisted. It was concluded that the origin of the noise is either internal to the dSPACE board or enclosed by the computer.

Since hardware solutions could not solve the noise problem, software filters were implemented directly at the analog input channels to smooth out the noise. In particular, 2nd order Butterworth filters were implemented. The following transfer function of the Butterworth filter was implemented using a cut-off frequency w_c of 100 rad/s:

$$H(s) = \frac{1}{(s/w_c)^2 + \sqrt{2}\,(s/w_c) + 1} \qquad (3.1)$$

The Butterworth filter is the filter type that results in the flattest pass band. The advantage of a 2nd order filter is that it gives better roll-off compared to a 1st order filter. Implementing the software filter at every ADC channel has significantly reduced the effects of noise on the data.

In fact, the resistance of the wire dropped during the transformation from martensite phase to austenite phase. This phenomenon disagrees with [**14**], the datasheet of NiTi properties published by SMA Inc. Further discussion and explanation will be given in Section 3.3.4.

3.3 Modelling Experiment

In control design, understanding and modelling of the properties of the actuator is invaluable as a design aid. This is especially the case for SMA actuators where there exists non-linearities and changes in properties such as electrical resistance during phase transformations.

The two-level relay controller of Grant based on his force and position models had been able to demonstrate that SMA actuators can be controlled accurately and rapidly but the concept of using safe current inputs represents a limitation. It is thus our research aim to use that as our basic control system and to further implement a mechanism that supplies and limits a greater amount of current to flow through the actuators for very short periods while preventing damage to the actuators.

The key to designing such a mechanism lies in examining and modelling the relationship between the input power, SMA resistance and contraction of the wire during phase transformation. A Simulink model had been designed to carry out this experiment.

3.3.1 Experimental Procedure.

The main objective of the experiment is to record and analyse the change in resistance values and displacement of the actuator wire during temperature variation and through phase transformation. Because there is no practical method of measuring the temperature of very thin Flexinol^{tm} wires in this project, a different state variable – the input power – of the actuator will be measured.

The following Fig 3.5 was set up in the experiment rig for the modelling experiment.

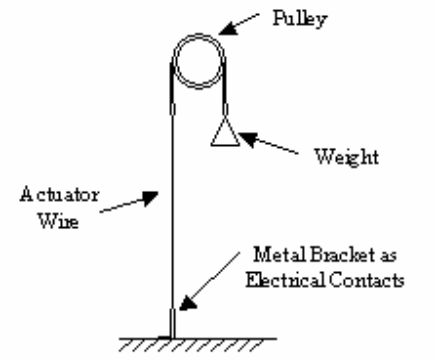

Figure 3.5 Experiment Set-Up for Modelling Experiment (Not to Scale)

The above set-up was used to measure during heating and cooling, the SMA profile of the main thermal cycle and the profile for any partial cycle of one wire actuator as a function of power. The procedure will be repeated with several values of loading using weights of 8g (sufficient mass to ensure tautness of wire), 50g, 100g, 150g and 200g. Between each cycle or experiment run, it is crucial not to re-initialise the encoder position. This ensured the correspondence between each experiment of different loadings and allows meaningful plotting of profiles as shown in Fig 3.9 and Fig 3.10.

For each case of loading, the experimental procedure was repeated using the following desired power profile:

- Fig 3.8 (a) for the main thermal cycle of the wire
- Fig 3.8 (b) for the partial or intermediate heating and cooling cycles of the wire
- Fig 3.8 (c) for both main and partial thermal cycles of the wire

A slow rate of change of the input power was used to ensure that the hysteresis profiles can be clearly observed and recorded.

3.3.2 Simulink Model.

The modelling experiment was implemented using the Simulink model shown in Fig 3.6 using a closed-loop feedback system. Features of the experiment model include the analog-to-digital conversion module with software filtering, encoder angle and wire contraction measurements as well as a Proportional-Integral (PI) controller to accurately track the desired input power.

The desired input power is programmed to have a maximum power P of 4.8 W according to the following equation:

$$P = I^2R \qquad (3.2)$$

where I is the input current to the SMA actuator and R the electrical resistance of the actuator. An input power of 4.8 W corresponds to a current level of 0.2 A (slightly higher than the safe level of 0.18 A to observe any additional contraction due to the higher current input) and a resistance value of 120 Ω. Profiles of the desired power are presented in Fig 3.8.

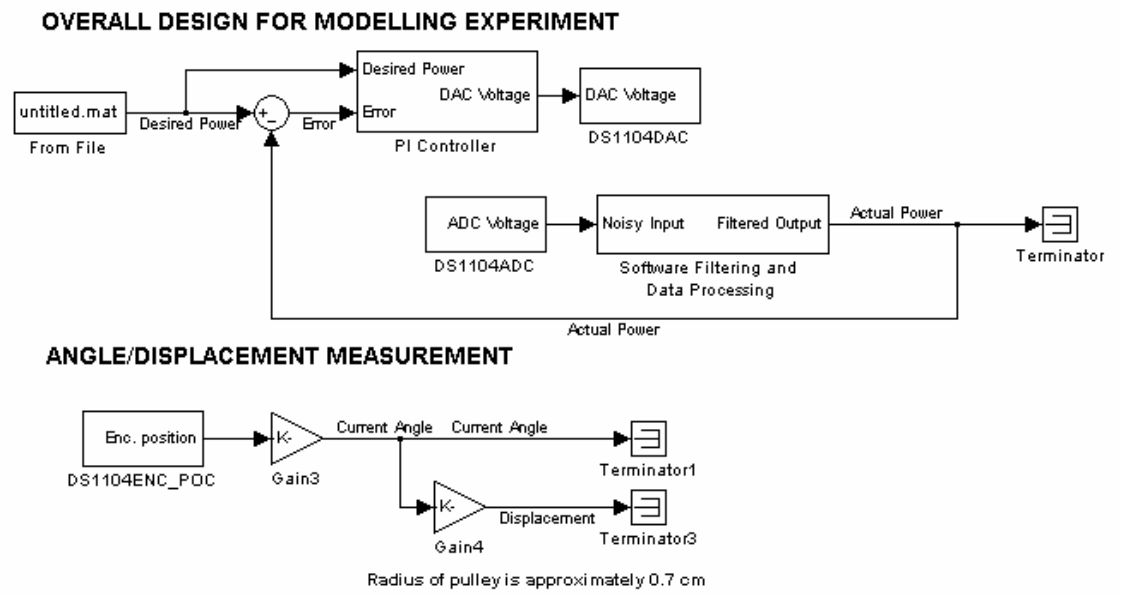

Figure 3.6 Simulink Model for Modelling Experiment

In a closed-loop feedback system, the response of the actual measured power can be different from the desired input power due to the varying of SMA physical properties such as its resistance. Therefore, it is necessary to ensure that the feedback controller is robust and provides exact tracking. A Proportional-Integral (PI) controller shown in Fig. 3.7 had been implemented for this purpose

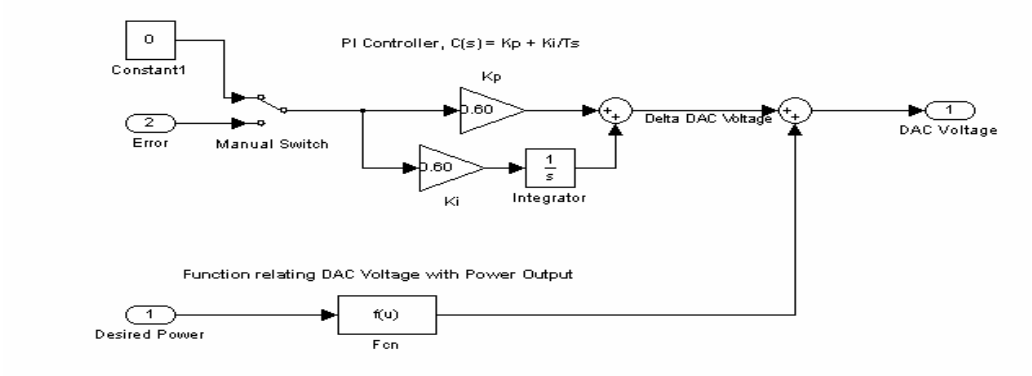

Figure 3.7 PI Controller for Modelling Experiment

3.3.3 Results.

Fig 3.8 presents the input power profiles that were used in the experiment to drive the Flexinol^{tm} wire actuator. A slow rate of input power at ± 0.1 Ws^{-1} was applied such that intermediate cycles in each main hysteresis curve can be recorded.

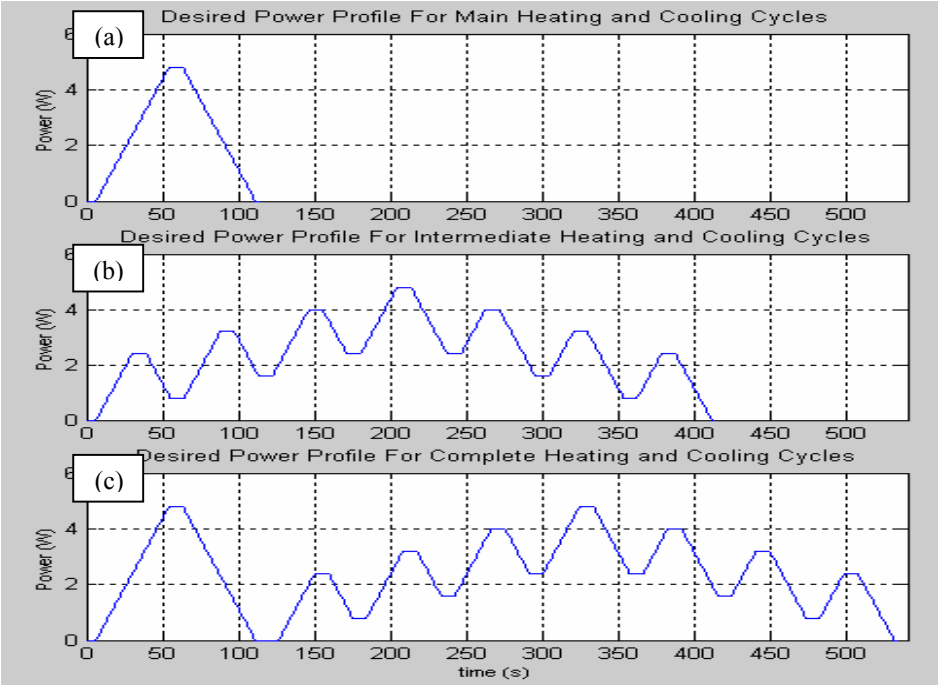

Figure 3.8 Desired Power Profile for Modelling Experiment. (a) For Main Thermal Cycle. (b) For Intermediate Thermal Cycles. (c) For Main and Intermediate Cycles.

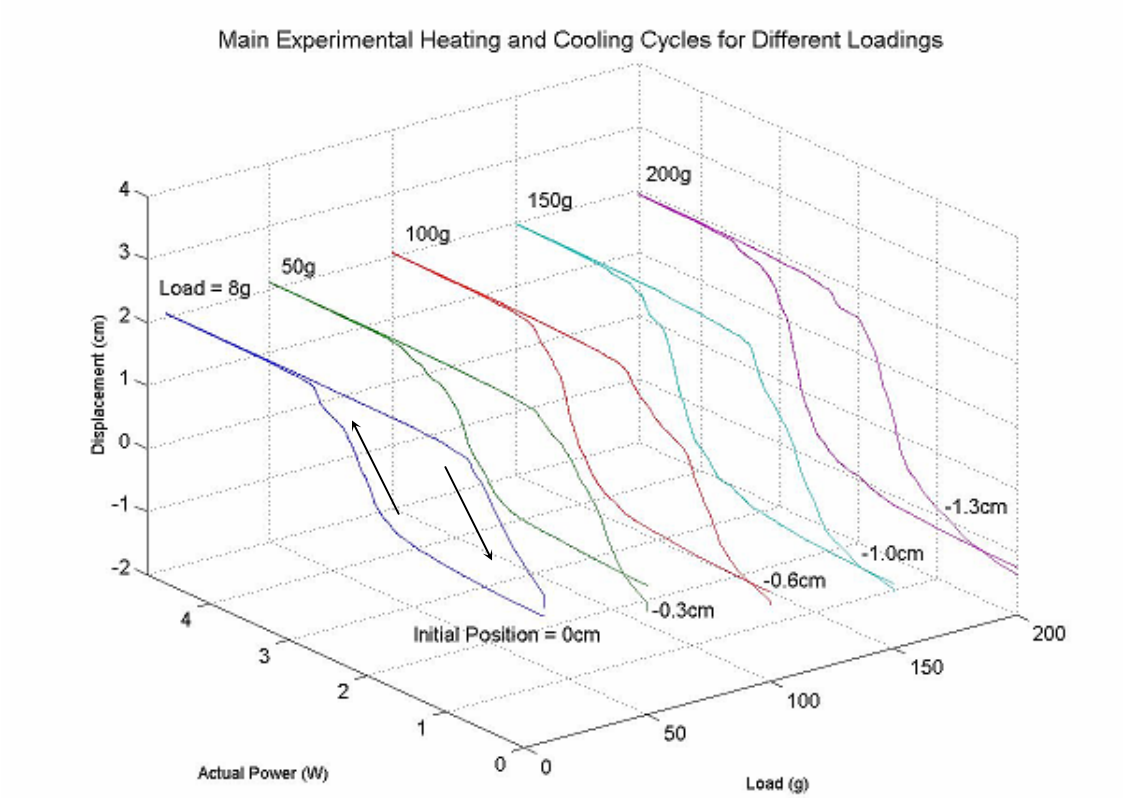

Figure 3.9 Hysteresis Profiles of Main Thermal Cycle with Different Loadings. (Using Input Power Profile of Fig 3.8(a))

Fig 3.9 presents the main thermal cycles of an SMA actuator wire when heated from the martensite phase and cooled from the austenite phase with different cases of loads. The input power profile of Fig 3.8 (a) was used. The arrow pointing upwards in the diagram corresponds to heating and the other arrow to cooling. It was observed that regardless of the amount of loads, the hysteresis curves are very similar. This suggested that a simple, perhaps linear relationship could be obtained for control purposes.

As mentioned, the encoder position of each experimental run was preserved after each load increase. It was observed from the diagram that the initial position decreased after each thermal cycle as the amount of load was increased. This suggested that creeping of the actuator wire occurred. However, the maximum displacements of the SMA actuator were consistently recorded to be 2 cm. This is a positive indication that regardless of creeping, the effective range of SMA actuation is always consistent with the condition that the actuators are undamaged.

The next diagram, Fig 3.10 shows the main hysteresis curve and partial curves of intermediate heating and cooling of the actuator wire.

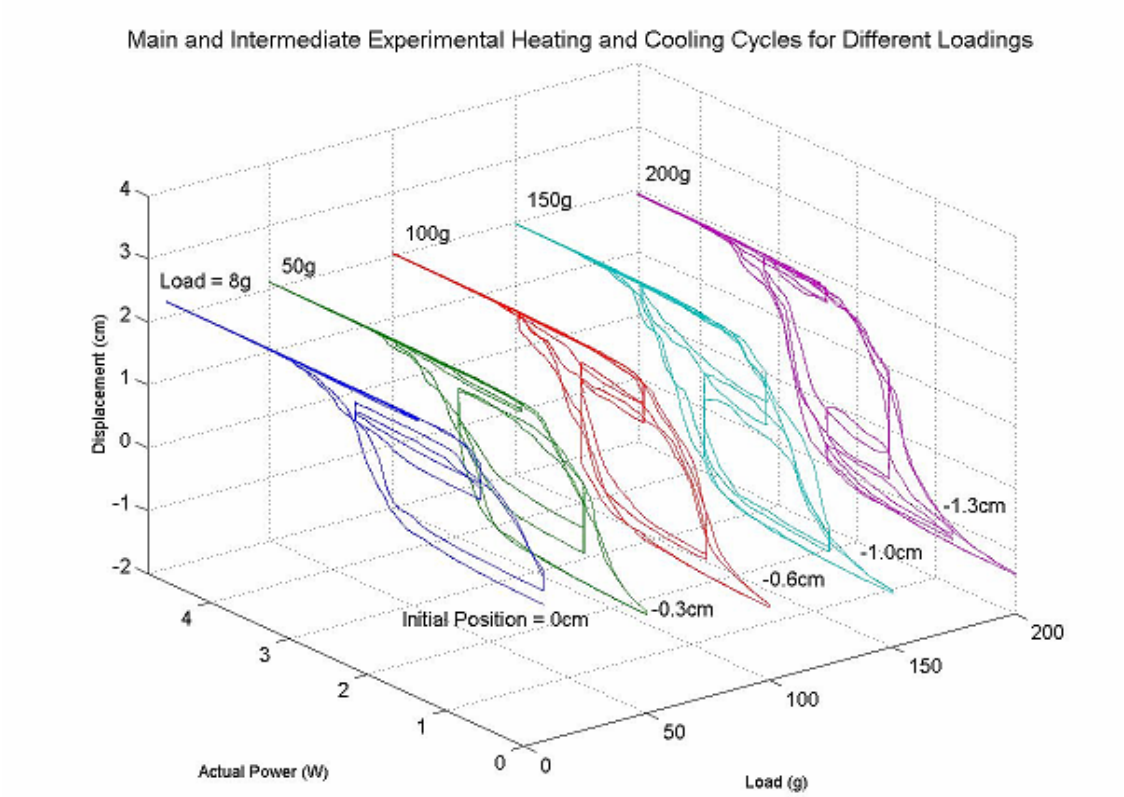

Figure 3.10 Hysteresis Profiles of Main and Intermediate Thermal Cycles with Different Loadings. (With Input Power Profile of Fig 3.8(c))

In Fig 3.10, the partial heating and cooling curves were observed to follow a specific trajectory. Most of the partial curves followed an almost horizontal trajectory until an input power sufficient to heat the actuator past the transformation temperature. It was observed that a steep change in the actuator displacement occurred only within a small range of input power.

The results suggested that a large actuation of the SMA wire within a short time could be achieved with a steep temperature increase. This significant temperature increase could be accomplished by supplying a very large input current to the actuators. A simple control mechanism based on this concept could be designed to achieve very fast motions from the SMA actuators.

To have aggressive motion, we need to improve Grant's relay controller to allow greater power consumption and thus higher current inputs. However, we also need to prevent the overheating and damaging of the SMA actuators. It is therefore hoped that a safety mechanism that clips the input to the actuators according to the power consumption history of the actuators could be implemented. The profiles above gave us information on the states of the actuators, whether they are in martensite phase, austenite or a combination of both. The temperature and martensite ratio of the SMAs could be estimated.

By looking at the resistance change of Flexinol^{tm} during thermal cycles, a better and simpler solution was devised. This mechanism allows dangerously high current inputs to pass through the actuators when the resistance value indicates that the actuator is not in the higher temperature austenite phase. On the other hand, if the actuator is austenitic, the mechanism limits the amount of power at a safe level.

3.3.4 Flexinol^{tm} Resistance Profile Discrepancy.

According to Table 2.1 [**14**], the resistivity for NiTi martensite is 80 micro-Ω cm and 100 micro-Ω cm for NiTi austenite. The electrical resistance of a wire, R is directly proportional to its resistivity, ρ according to the Equation 3.3:

$$R = \rho \frac{L}{A} \qquad (3.3)$$

where L is the length of the wire and A the cross-sectional area of the wire. The length of Flexinol^{tm} wires used for actuation is 1 meter and the diameter is 100 micron (0.004 inch). Assuming that changes in length and diameter are negligible during phase transformation, the resistance for Flexinol^{tm} martensite is approximately 99 Ω and for austenite, 123 Ω. This indicates that the resistance value of Flexinol^{tm} increases as it undergoes a phase transformation from martensite to austenite. However, the resistance profiles obtained in this work are clearly different to the values from the datasheet.

Fig 3.11 presents the electrical resistance profile obtained during the main thermal cycle from the modelling experiment. The data had been processed with 2nd order Butterworth filters to smooth out the noise. The kinks or distortions on the graph were results of the PI controller attempting to track the desired power exactly.

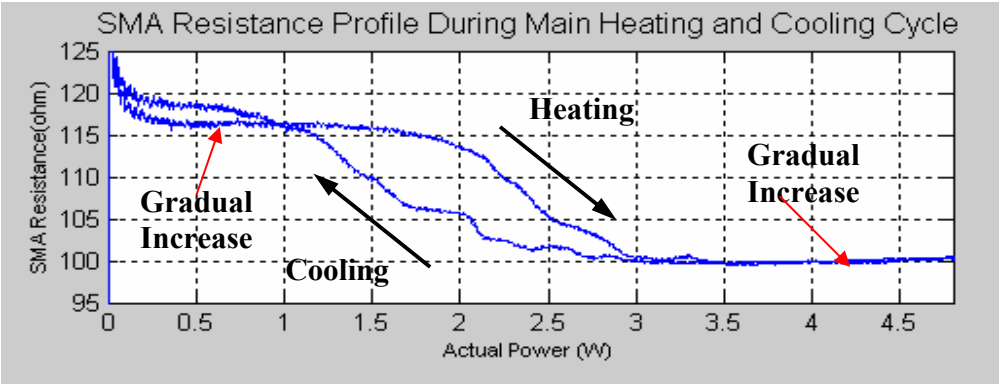

Figure 3.11 Flexinol^{tm} Resistance Profile During Main Thermal Cycle (With Distortion).

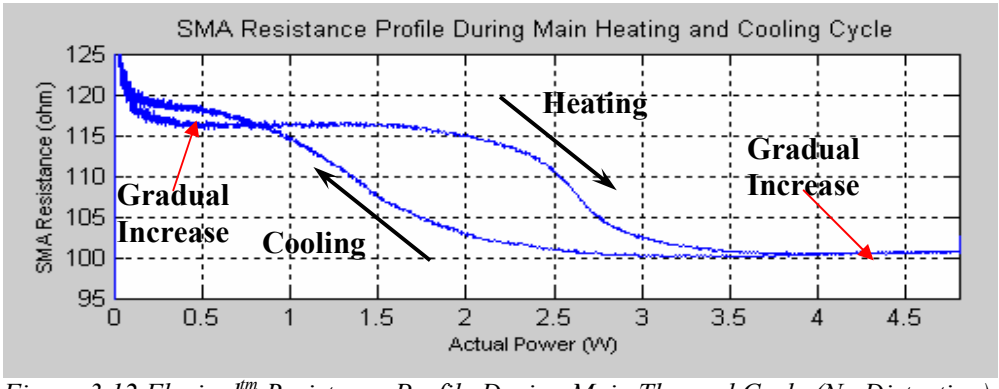

Figure 3.12 Flexinol^{tm} Resistance Profile During Main Thermal Cycle (No Distortion).

Fig 3.12 above presents the resistance profile during the main thermal cycle with software noise-filtering as well. The Simulink model in this case does not have a PI controller but instead, implements the ramp input of Fig 3.2 and measures its power using the ADCs. As observed, kinks were not present anymore in this profile.

Both graphs have the following similar features:

- Before phase transformation to austenite, there was a gradual increase in resistance with the power, and thus, with temperature. The average range was observed to be approximately between 115 – 116 Ω and was consistent across all experiment runs.
- During the transformation to austenite, resistance dropped to approximately 100 Ω.
- As power (temperature) increased, a gradual increase in the resistance was again observed. The observed range was between 100 – 102 Ω and was again consistent with all the results obtained.
- During the transition back to martensite, the resistance increased to 120 Ω.

According to [**8**], the relationship between temperature and resistivity for metals in general, is fairly linear over a broad temperature range. Therefore, the gradual increase in resistance during the rise in power (temperature) without phase change is a typical characteristic of metals.

However, there is a clear discrepancy between the obtained results and [**14**]. The results in this work indicated a fall of the electrical resistance of Flexinol^{tm} wire during the phase transformation from martensite to austenite. This clearly disagrees with the datasheet.

However, other literature and sources support results obtained in this work. Researchers such as Kotil, Sehitoglu, and Chumlyakov in [**9**], Mosley, Mavroidis and Pfeiffer in [**11**] and Serneels in [**13**] have similar results. This strongly suggests that the results of this work are correct. The datasheet is either wrong in its resistivity values or it is referring to another aspect of the SMA.

3.4 Chapter Summary

Because the experimental set-up had been uniquely designed and constructed for this work, it has to be understood and checked thoroughly. This chapter provided an overview of the pertinent hardware and software features and procedures that formed the logical steps towards a complete control system. The modelling experiments carried out had been able to provide information especially on the electrical resistance values of the SMA wires that are useful in designing an improved control system. It is hoped that all the results obtained could be examined in the future to fully estimate the temperature and martensitic ratio of the SMA wires.

The next two chapters will deal with the control systems that have been implemented and substantially experimented in this work.

Chapter 4: Two-Level Relay Controller System

Based on the results of the modelling experiment in Chapter 3, the power limiter mechanism has been developed. Before examining the performance of this improved control system, we will first look at the performance of Grant's two-level relay controller in this chapter.

Chapter 4 will set off with a discussion of general control design issues including the difference between the 'no load' system and the system with additional loads. Section 4.2 presents a description of Grant's two-level relay controller and its implementation. Results of the closed-loop performance of the controller for the 'no load' case are also presented in Section 4.3. In section 4.4, the position control of the system with an additional load will be examined.

4.1 General Control Design

According to [**1**], the response time of SMA actuators is one of the critical characteristics that must be carefully analysed and optimised in order to create aggressive motion control. As observed in Chapter 3, the response of the SMA wire is inherently influenced by the wide hysteresis loop present as well as the slow cooling rate, thus introducing a relatively slow response during phase change.

The antagonistic arrangement of the actuators aims to eliminate the above problem. It also increases the range of actuation to twice the range of using a single actuator. However, due to slack in the wires, the effective range of the actuators has been compromised. Section 4.1.1 will address this problem and provide a better solution.

Section 4.1.2 discusses the usage of SI units to communicate between each part of the control system. This concept will be used across all Simulink control design models in this chapter.

To prevent overheating the Flexinol^{tm} wires and damaging the shape memory effect, it is necessary to ensure that only one actuator is driving the system at a time. This is one of the incentives of implementing relay control to the system. The relay controller will be further addressed in Section 4.1.3. The difference between a 'no load' system and a 'with load' system will be discussed in Section 4.1.4.

4.1.1 Slack in Wire Actuators.

As mentioned in Section 3.1, the procedure of fixing the wires in the rig resulted in significant slack that had decreased the effective range of actuation. The further the actuation moves from the neutral position, the longer the wire needs to contract. Due to limited percent strain of the wire, the range of actuation is limited.

On the other hand, it was also noted that the slack should not be eliminated entirely to prevent vibration in the system caused by the coupling of the antagonistic wire pairs. This was experimented and observed. Vibration occurred when the contraction of one wire being heated caused the other

wire in the antagonistic pair to act like a spring load. It may also cause the passive wire to try to stretch beyond its strain recoverable length. This would permanently damage the SMAs.

As a compromise, the pulley was rotated to an angle of 80° from the neutral position compared to the original 100° before clamping the wires permanently. The effective actuation range has increased to ±60° instead of the original ±30°.

4.1.2 Control System Language.

It is often good practise to ensure that the modules of a control system communicate using an internal language of SI units, such as amperes, ohms, watts and meters. This allows future researchers to understand the Simulink models and designs in this work and continue with the research.

Conversion from the internal language to an external language such as the DAC voltage, of the experimental set-up in this work should be completed at the final stage before sending the signals to the DAC channels. When receiving signals from ADC channels, conversion to SI units should be conducted first before passing the data to the control system.

All control system models in this chapter and the next are designed using this principle.

4.1.3 Relay Control.

A relay control system is also known as an ON-OFF system. In this work, current is applied to one actuator at a time using the relay controller. According to [**6**], the use of relay control together with the antagonistic arrangement of the SMA actuators simplifies the control design as the problem of hysteresis in the input-output relations of actuators is transformed to a problem of delay.

The simplest relay controller consists of switching on one actuator while switching off the other in the antagonistic arrangement, and vice versa, depending on the direction of the desired actuation. Using the safe current input, I_{safe}, to prevent damaging the actuators, the output of the controller is given by:

$$y = \begin{cases} I_{safe} & \text{for } \varepsilon > 0; \\ - I_{safe} & \text{for } \varepsilon < 0, \end{cases} \tag{4.1}$$

where y is the current input to the plant (actuators) and ε the error of the controlling variable which in this work is the encoder angle error. This relay control is considered ideal without hysteresis and has infinitely fast switching. This is also the most efficient and fastest way to drive the plant to a desired setpoint since the highest input is used at all times.

The main disadvantage of using maximum input for high speed switching is stability degradation. Once the setpoint is reached, the maximum input will cause the system to have large magnitude hunting error, or limit cycle, or to go unstable. To reduce this effect, Grant proposed to use a two-level relay controller. This will be further discussed in Section 4.2.

4.1.4 Load/Inertia Issues.

It is important to observe and compare the responses of the system using a control design in two cases – the ‘no load’ case and the ‘with load’ case. The ‘no load’ case is the situation where no load will be additionally coupled to the existing system. Recall that the actuators are coupled to the

encoder disk by a small pulley. The inertia of this pulley and the shaft together with the encoder disk constitutes the inertia of the existing system for the 'no load' case.

As for the 'with load' case, a small copper rod with a mass of 40 g is coupled to the shaft and the pulley on the experiment rig shown in Fig 2.6. The copper rod constitutes a difficult load to control, as there is no additional damping in the system. With the additional load, the performance of the controller will be expected to degrade due to an increased limit cycle magnitude.

A limit cycle is the vibration, or oscillation of a system that, once initialised, will continue or operate independently of the starting conditions and other moderate disturbances that tend to slow the process down or speed it up[1].

4.2 Danny Grant's Two-Level Relay Controller

In this section, the position control of a pair of antagonistic SMA actuators will be examined for both the 'no load' and the 'with load' cases but first, the design and the implementation of the two-level relay controller will be considered.

4.2.1 Design Issues.

Compared to a simple relay controller with one level of input, the two-level relay controller uses two constant magnitude current inputs. As mentioned, depending on the sign of the angle error, one actuator of the antagonistic pair is driven to provide tracking. When the angle error is high, the high current value, I_H, is used to drive the plant quickly to the setpoint. As the angle error approaches zero and reaches the boundary layer, λ, the relay controller switches to a lower current input, I_L, to minimise the limit cycle magnitude. The advantage of this multi-level relay control is smoother and more stable response together with the benefit of fast response.

The following equation represents the input-output relationship of the controller:

$$y = \begin{cases} I_H & \text{for } \lambda \le \varepsilon; \\ I_L & \text{for } 0 \le \varepsilon < \lambda; \\ -I_L & \text{for } -\lambda < \varepsilon \le 0; \\ -I_H & \text{for } \varepsilon \le -\lambda \end{cases} \qquad (4.2)$$

In Equation 4.2, y is the current input to the plant (actuator), the positive values of the current inputs correspond to one actuator and the negative values to the other. The magnitude of I_L needs to be sufficiently high to maintain the temperature of the actuator and its contraction at the setpoint.

The design parameters for this controller are the magnitudes of the current inputs, I_H and I_L, as well as the error boundary layer, λ, for switching between the high and low currents. Block diagrams

[1] Definition obtained from the Web Dictionary of Cybernetics and Systems at http://pespmc1.vub.ac.be/ASC/LIMIT_CYCLE.html, accessed on 17th June 2003.

of the two-level relay controller as well as the interpretation of the current inputs are graphically shown in Fig 4.1 (Adapted from [**6**]).

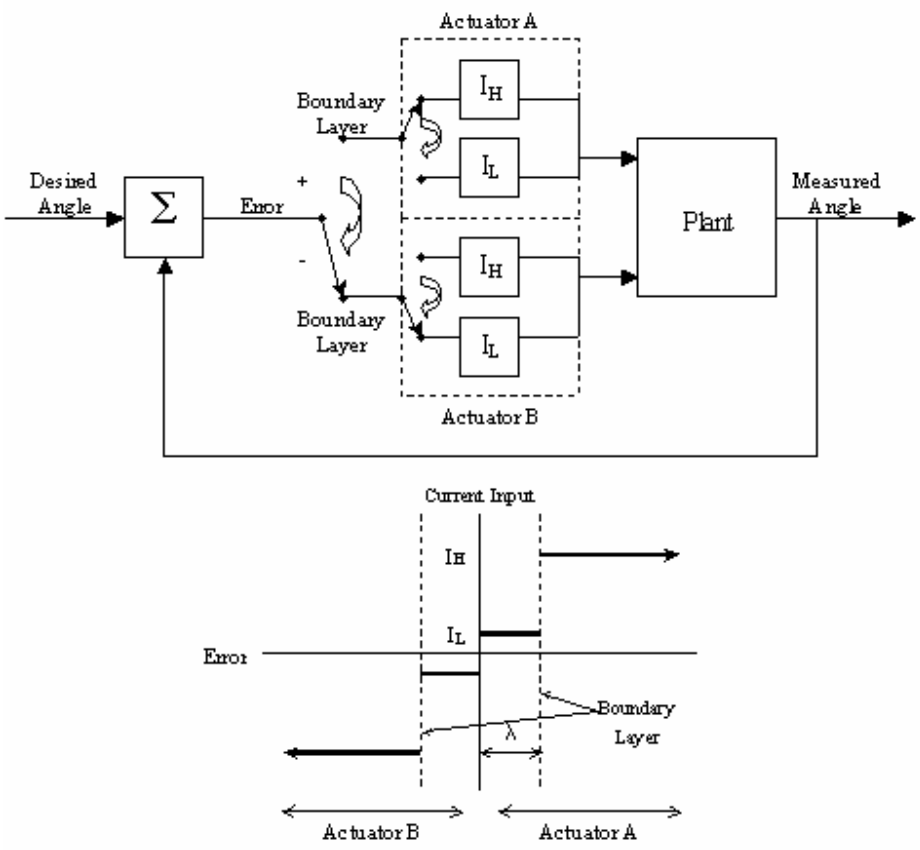

Figure 4.1 Two-Level Relay Controller

The two-level relay controller in this work uses the maximum safe current input of 0.18 A as I_H and a lower current input of 0.12 A as I_L. A boundary layer of ±0.5° is used throughout Chapter 4 The step and tracking responses of this controller will be presented.

4.2.2 Implementation.

The complete Simulink models of Grant's Two-Level Relay Controller are presented as Fig C.6 and C.7 in Appendix C. The actual duration of each real-time experiment using the control system lasted 30 seconds. There are two phases in each experiment. The first is the initialisation phase of the encoder module using the index pulse as discussed in Chapter 3. Once the index position has been detected and the encoder angle set to zero, the control phase commences using the proposed two-level relay controller.

4.3 Position Control – No Load

The experimental responses to a series of step inputs as well as sine inputs for the 'no load' case are examined in this section.

4.3.1 Step Response of Two-Level Relay Controller.

Fig 4.2 presents the results obtained from the two-level relay control system to step inputs. Looking first at the complete 30-second step responses to desired steps of ±30° and ±45° of Fig 4.2 (a) and (b), the initialisation phase takes place in the first 8 seconds. During this phase, the encoder angle is set by the control system to remain at 0° until the control phase commences from the 8th second to the end of the experiment. Figures from Fig 4.3 onwards will omit the initialisation phase responses.

Fig 4.2 (c) and (e) presents a detailed view of the step response to a ±30° step input. In terms of time-domain specification, the average rise and fall time to this step input was approximately 0.35 seconds. For the response to a ±45° step input shown in Fig 4.2 (f) it was slightly longer and requires approximately 0.45 seconds. This is expected as the setpoint is further away from the neutral position, so it takes a longer time for the system to reach the desired setpoint. Note that there was no significant overshoot in both step responses due to the controller switching to the I_L current level at the boundary layer. This effectively slows down the contraction of the wire and reduces the overshoot.

The limit cycle can also be seen for both response in Fig. 4.2 (g) and (h). Due to the inertia of the existing system as well as the inherent nature of the switching relay controller, limit cycles were present in the steady state responses. The frequency of the limit cycle was approximately 55 Hz in Fig 4.2 (g) and 60 Hz in Fig 4.2 (h). The magnitude of the limit cycle varies throughout the different step inputs, increasing from smaller to larger steps. The following Table 4.1 summarises the limit cycle magnitudes of responses to varying step inputs.

Step Input (°)	Peak-to-peak Magnitude of Steady State Limit Cycle (°)
±15	0.05
±30	0.20
±45	0.30
±60	0.50

Table 4.1 Limit Cycle Magnitudes for 'No Load' Step Responses.

There was an increasing trend in the magnitude as the actuation range was increased. The antagonistic setting of the actuator wires acts like a mass-spring system. When an actuator is contracted to reach a desired setpoint, the other actuator is stretched and acts like a spring. The increased limit cycle magnitude observed was due to the greater biasing force from the antagonistic actuator when the setpoint was further from the zero-position.

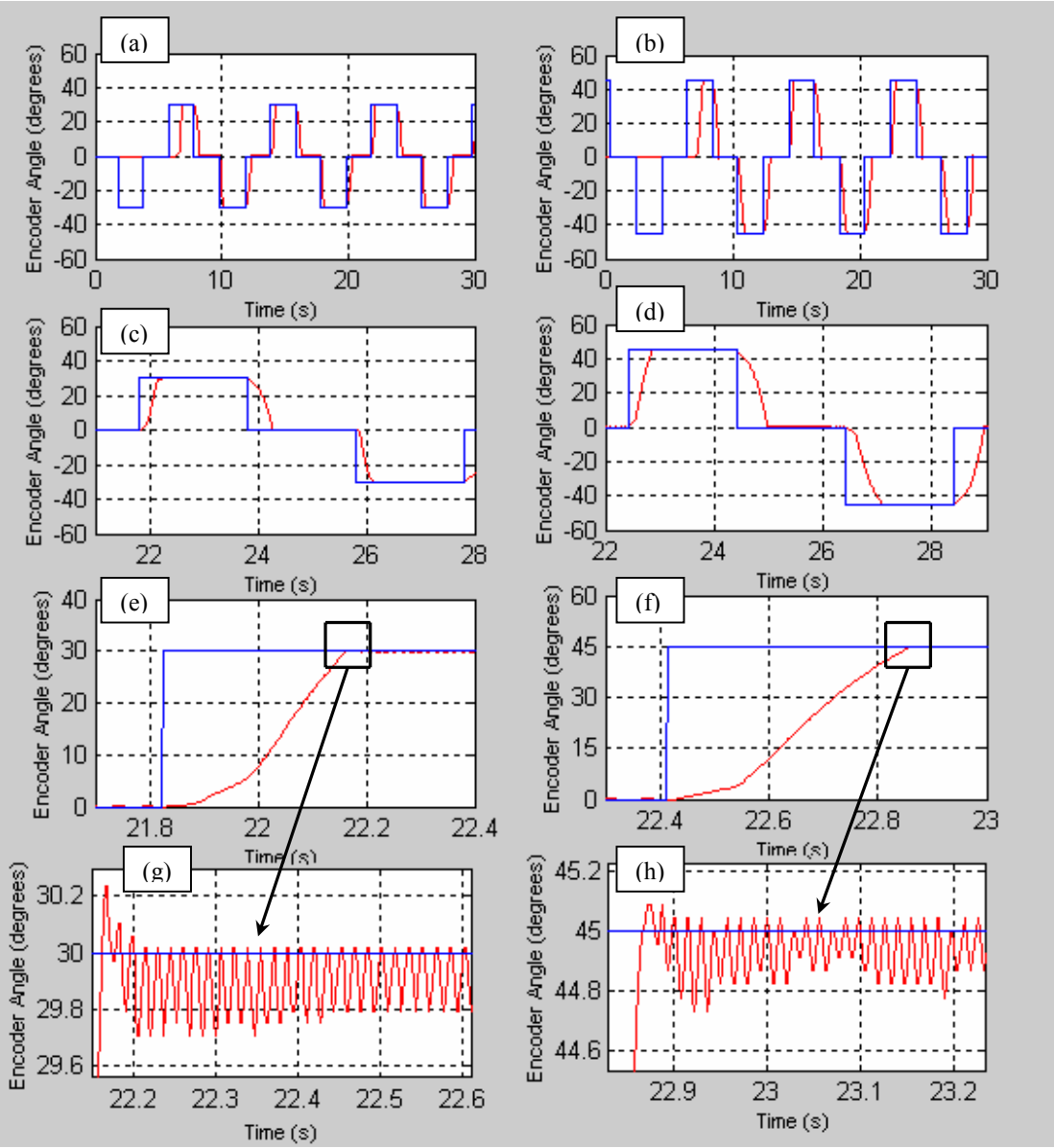

Figure 4.2 Closed Loop Position Step Response Using Two-Level Relay Controller for a pair of SMA Antagonistic Actuators (No Load Case): Blue Line = Desired Angle; Red Line = Actual Angle.
(a) Full Step Response (Initialisation and Control Phase) to Input of ±30°.
(b) Full Step Response (Initialisation and Control Phase) to Input of ±45°.
(c) Closer View of Response from (a). (d) Closer View of Response from (b).
(e) Detailed Response from (a). (f) Detailed Response from (b).
(g) Limit Cycle for Response from (a). (h) Limit Cycle for Response from (b).

4.3.2 Tracking Response of Two-Level Relay Controller.

Fig 4.3 presents the tracking responses of the system to a series of sine inputs of 45° amplitude, with varying frequencies of 0.2 Hz, 0.25 Hz, 0.33 Hz and 0.5 Hz. It should be noted that the initialisation of the encoder had been conducted for each case but had not been shown in Fig 4.3.

First, by examining the experimental response of Fig 4.3 (a), it can be seen that the tracking for the 0.2 Hz wave was accurate. A small limit cycle was observed around the setpoint when examined in detail, as shown in Fig. 4.3 (b). As the frequency of the sine wave increased, the system began to lag behind the desired response as seen in Fig. 4.3 (c) and (d) due to the speed of response of the actuators. This is because it takes a finite amount of time for the actuators to contract or relax according to the input current. It can be seen in Fig 4.3 (e) and (f) that tracking was no longer accurate for the 0.5 Hz sine wave.

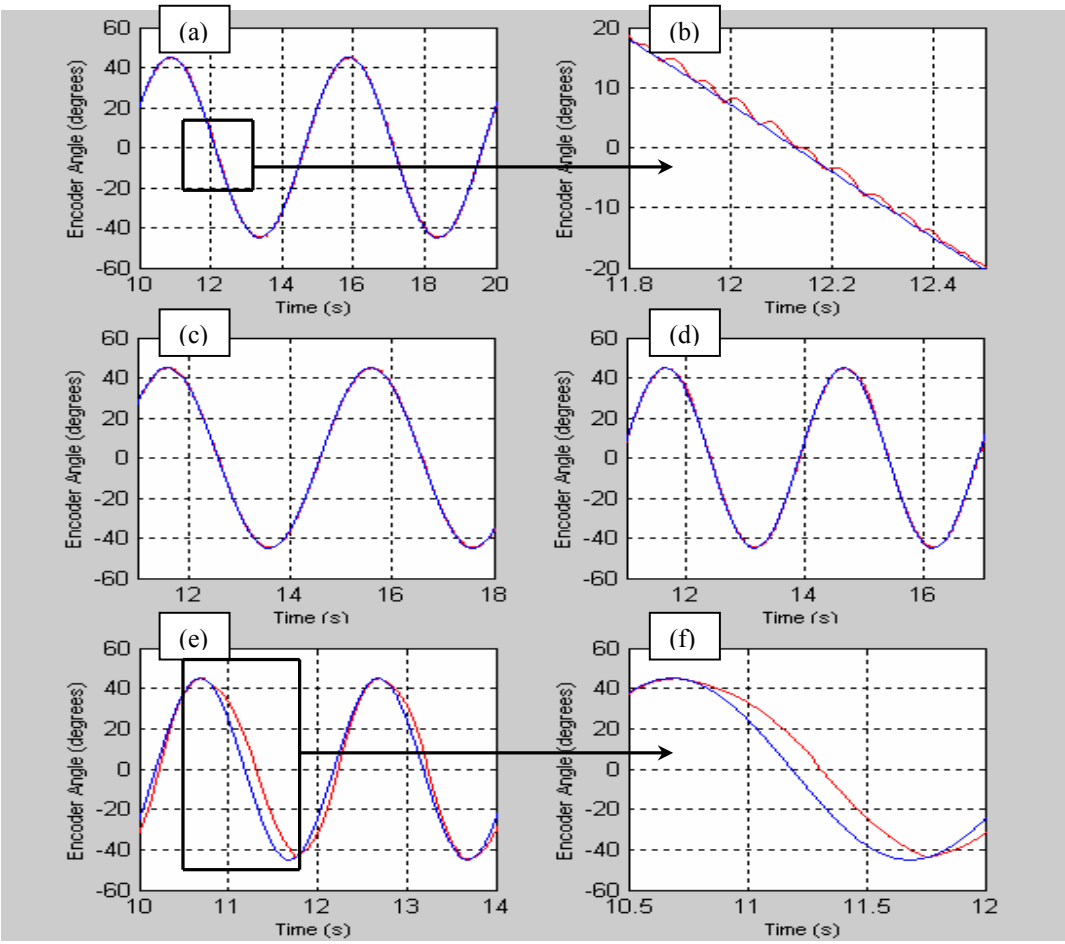

Figure 4.3 Close Loop Position Sine Response (Asin(2πft)) Using Two-Level Relay Control for a pair of SMA Antagonistic Actuators (No Load Case): Amplitude = 45°; Blue Line = Desired Angle; Red Line = Actual Angle.
(a) Sine Response with f = 0.2 Hz. (b) Detailed Sine Response of (a).
(c) Sine Response with f = 0.25 Hz. (d) Sine Response with f = 0.33 Hz.
(e) Sine Response with f = 0.5 Hz. (f) Detailed Sine Response of (e).

The experimental tracking errors for the sine waves in Fig 4.3 are shown in Fig 4.4. Again, note that the initialisation phase had not been shown.

As can be seen in Fig 4.4 (a) and (b), the errors for the 0.2 Hz and 0.25 Hz sine waves revolved around the boundary layer width of ±0.5° used in the two-level relay controller. The maximum error observed in these two curves occurred when the actuators were at their peak velocity at the zero position. As for the tracking error of the 0.33 Hz sine wave shown in Fig. 4.4 (c), the sudden rises in error observed occurred right after the sine wave peaks. This phenomenon occurred when the controller switched from I_L to I_H attempting to track the sine wave. Delays occurred as the actuator required a duration of time to achieve sufficient temperature in order to begin contracting. Fig 4.4 (d) presents the error of the inaccurate tracking for the 0.5 Hz sinusoidal input.

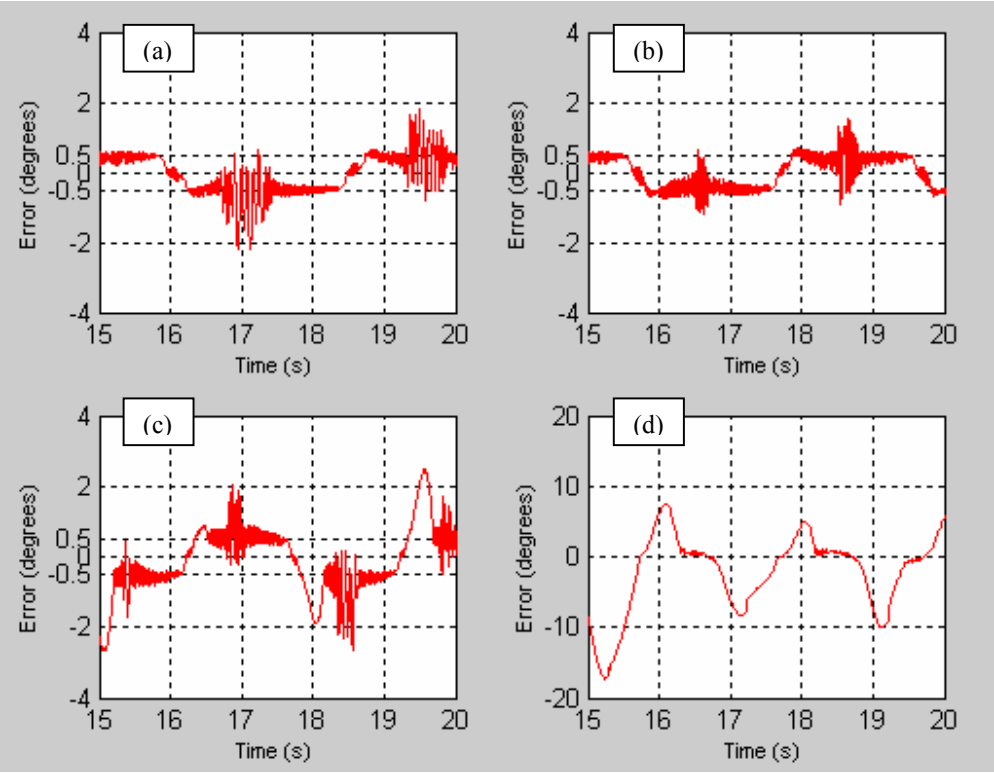

Figure 4.4 Tracking Error for Sine Responses (Asin(2πft)) from Fig 4.3. (a) f = 0.2Hz. (b) f = 0.25 Hz. (c) f = 0.33 Hz.. (d) f = 0.5 Hz.

4.4 Position Control – With a Load

This section examines the effects of an additional copper rod in the system on the two-level relay controller. The response of the antagonistic pair of actuators to a series of steps with an extra load of 40 g is shown in Fig. 4.5. The relay-controller managed to track the step inputs but the limit cycles had degraded significantly compared to situations of 'no load'.

Fig 4.5 (a) and (b) show the experimental responses to a step input of ±30° and ±45° with the initialisation phase omitted. A close up of the responses are shown in Fig. 4.5 (c) and (d). Fig. 4.5 (e) and (f) presents a detailed view of the limit cycles. With the added load, the frequency of the limit cycles had decreased to approximately 6 Hz but the magnitude had increased drastically. This was due to the inertia of the load.

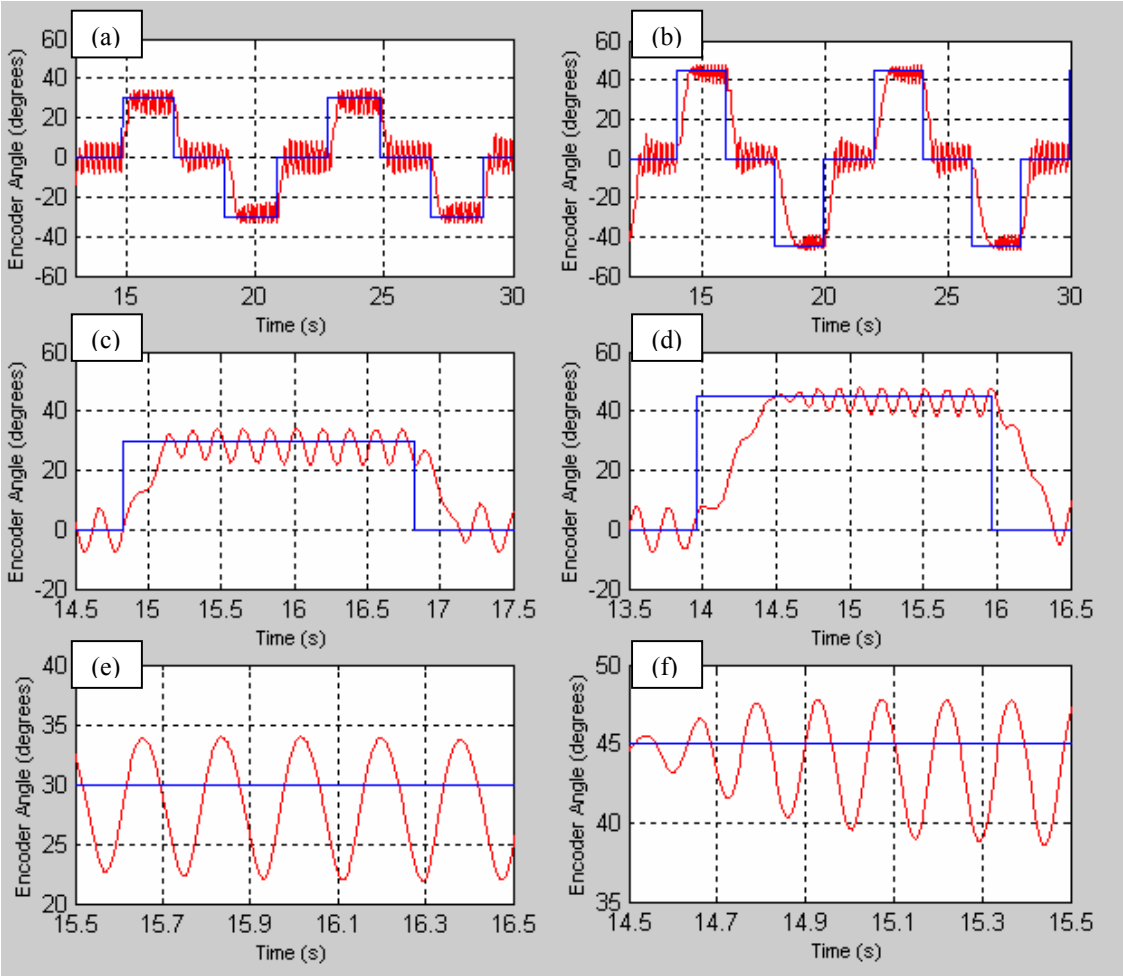

Figure 4.5 Close Loop Position Step Response Using Two-Level Relay Controller for a pair of SMA Antagonistic Actuators (With Load Case): Blue Line = Desired Angle; Red Line = Actual Angle.
(a) Step Response to a Desired Input of ±30°. (b) Step Response to a Desired Input of ±45°. (c) Detailed Response from (a). (d) Details Response from (b).
(e) Limit Cycle for Response from (a). (f) Limit Cycle for Response from (b).

4.5 Chapter Summary

In this chapter, Danny Grant's two-level relay controller design had been discussed and implemented to examine the experimental responses to both the 'no load' and the 'with load' cases.

For the 'no load' case the two-level relay controller was found to be accurate and rapid. The step responses were seen to go into a low magnitude limit cycle at setpoints. The tracking responses to a series of sine waves were also shown to be accurate at frequencies of 0.2 Hz and 0.25 Hz. However, at higher frequencies such as 0.5 Hz, the system began to lag behind the desired input.

For the 'with load' case, the additional load degraded the performance of the relay controller. The magnitude of the limit cycles had been observed to increase significantly.

So far, the two-level relay controller had implemented a safe current of 0.18 A as I_H with the aim of preventing damage to the actuators. The downside of this is the compromising of the speed of the response as was seen in the tracking responses at higher frequencies. Although the rise time of step responses was less than 1 second, this time-domain specification can still be improved.

Chapter 5: Improved Relay Controller System with Power Limiter Mechanism

This chapter presents the design of the power limiter mechanism and its implementation in addition to Grant's relay controller. Similarly, results will be examined for both the 'no load' system and the 'with load' system. Comparisons of control system performances will be made in Section 5.4.

5.1 Relay Controller with Power Limiter Mechanism

5.1.1 Power Limiter Mechanism Design.

While the two-level relay controller performed adequately for the step inputs with no load as well as the sine inputs at frequencies less than 0.5 Hz, its performance can be improved. The main reason for implementing the power limiter mechanism in addition to the two-level relay controller in the control system is to increase the speed of actuation by allowing greater power input.

By looking at the responses of the plant to a step input in Fig 5.1, it is very clear that higher magnitude of current inputs increases the speed of response. Therefore, by controlling the level of power input to the system, we can allow greater current inputs through the wire actuators as well as to limit it to prevent damage to the wires. The amplifier circuit and the power supply unit had been specifically chosen for this purpose - very high power consumption of up to 30 Watts. The responses of Fig 5.1 were obtained using the two-level relay controller by varying I_H, the high current level.

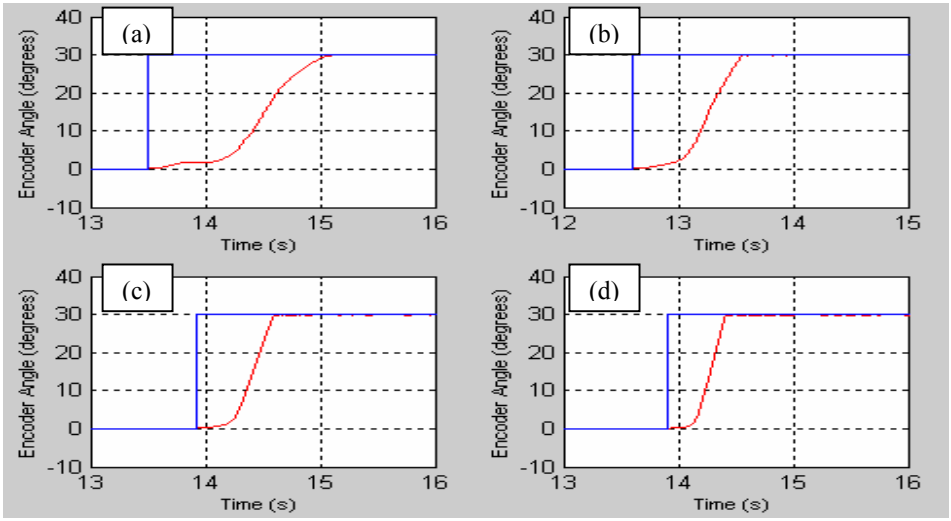

Figure 5.1 Response to Step Input with Varying Current Inputs: Blue Line = Desired Angle; Red Line = Actual Angle. (a) Current Input of 0.14 A. (b) Current Input of 0.16 A. (c) Current Input of 0.18 A. (d) Current Input of 0.20 A.

As discussed in Chapter 3, the resistance values allow the prediction of the phase of the Flexinol^{tm} wire. The following scheme is proposed to implement the power limiter mechanism. This scheme uses the measured electrical resistance of the Flexinol^{tm} wires to either allow greater power input or limit the power to a safe value.

There are four power limiter design variables - the resistance thresholds of the actuator in martensite phase and in austenite phase, R_{mar} and R_{aus}, the maximum safe, continuous power for the actuator, W_{safe}, as well as the maximum power that the amplifier can deliver to the actuator, W_{amp}.

When the resistance of the wire is measured as R_{aus} (the resistance at fully austenite phase), the mechanism limits the power input at W_{safe} to prevent overheating the wire. The W_{safe} power level corresponds to the safe current level of 0.18 A. As the wire cools, its resistance increases, thus allowing the mechanism to permit higher power inputs into the actuator. The maximum power that can be sent to the actuator is determined by the control system. If the resistance is measured at R_{mar}, the control system allows W_{amp} to be delivered to the actuator.

Fig 5.2 presents a graphical interpretation of the power limiter scheme.

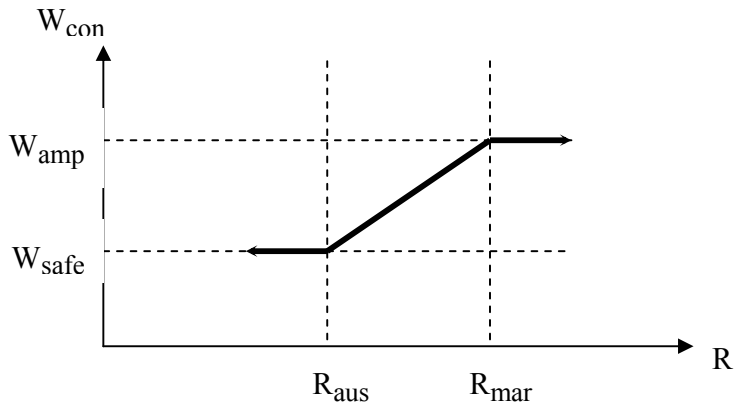

Figure 5.2 Power Limiter Mechanism

The equation for this mechanism is described in Equation 5.1.

$$W_{con} = \begin{cases} W_{safe} & \text{for } R < R_{aus}; \\ W_{safe} + (W_{amp} - W_{safe}) \times \dfrac{(R - R_{aus})}{(R_{mar} - R_{aus})} & \text{for } R_{aus} \le R < R_{mar}; \\ W_{amp} & \text{for } R_{mar} \le R, \end{cases} \qquad (5.1)$$

where W_{con} is the maximum power that the control system is allowed to send to the actuator and R the measured electrical resistance of the actuator. Another condition which is not specified in Equation 5.1 is that once the response enters λ, the relay controller boundary layer, the power limiter mechanism automatically shuts down and only I_L is delivered.

5.1.2 Implementation.

The Simulink model of the closed loop feedback control system with the power limiter mechanism is given as Fig C.8, C.9 and C.10 in Appendix C. Again, note that there are two phases recorded in the actual experimental responses but for all of the graphs presented in the following sections, the initialisation phase has been omitted.

The next sections present results of the control system to a series of step and sine inputs in the 'no load' case as well as step responses for the 'with load' case.. Comparison of performances between Grant's relay controller as well as the improved controller with power limiter mechanism will be made at the end of the chapter.

5.2 Position Control – No Load

5.2.1 Step Response of Control System with Power Limiter.

The improved control system implements a manual switch that controls the power limiter mechanism. When switched off, the control system functions exactly like Grant's two-level relay controller. Therefore, direct comparison can be made between the responses by switching on .the power limiter mechanism. Fig 5.3 presents this implementation. Between the duration from the 20th to the 32nd seconds, the two-level relay controller was implemented. The next thirteen seconds are responses with the power limiter mechanism switched on.

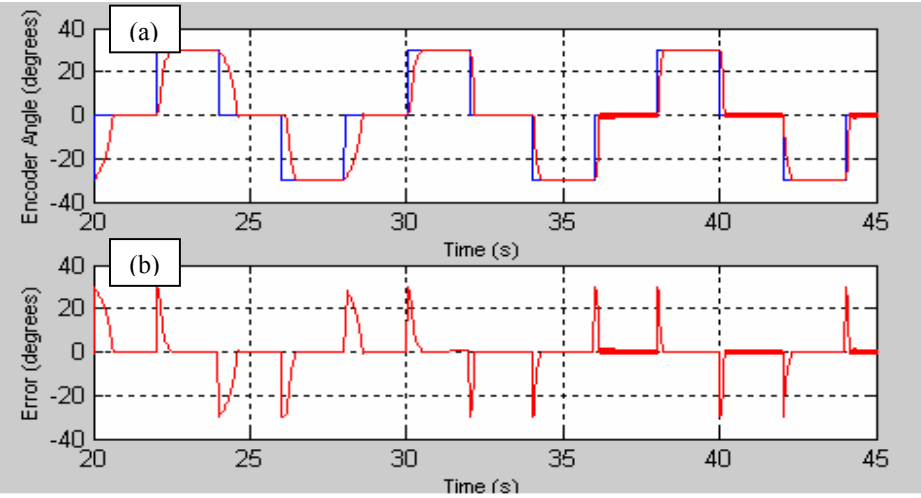

Figure 5.3 Comparison of Step Responses between Grant's Two-Level Relay Controller and the Relay Controller with Power Limiter Mechanism (No Load Case): Boundary Layer, $\lambda = \pm 0.5°$; Blue Line = Desired Angle; Red Line = Actual Angle; Response of 20-32 s = Power Limiter OFF; Response of 32-45 s = Power Limiter ON. (a) W_{amp} = 15 W; R_{aus} = 105 Ω; Desired Step of ±30°. (b) Angle Error from Response (a).

The figure above clearly shows that the rise and fall times of the step response had decreased significantly once the power limiter was switched on. In terms of limit cycles, the performance of step response is slightly worse off using the power limiter mechanism at the steady state. Because the control system pumps higher level of current into the actuators, the speed of the actuators is higher.

As the plant approaches the boundary layer of the relay controller, the response is such that even if switched to I_L, larger overshoots occur due to the higher momentum of the system. The result is, the response does not converge within the boundary layer.

The next figure, Fig 5.4 provides a clear indication of the successful functioning of the power limiter mechanism. This figure represents the input power and SMA resistance profiles of the system when the experiment of Fig 5.3 was carried out.

By examining Fig 5.4 (a) and (c) first, it is clear that very large amount of input power determined by the control system had been delivered when needed. Before the power limiter mechanism kicked in, the relay controller delivered only a safe amount of input power (less than 5 W) to the actuators. When switched on at the 32nd second, if the angle error is greater than λ, the boundary layer, a large input power was delivered into the actuators alternatively as observed in Fig 5.4 (a) and (c). The effect of this was clearly shown by the reduction in rise and fall times in Fig 5.3.

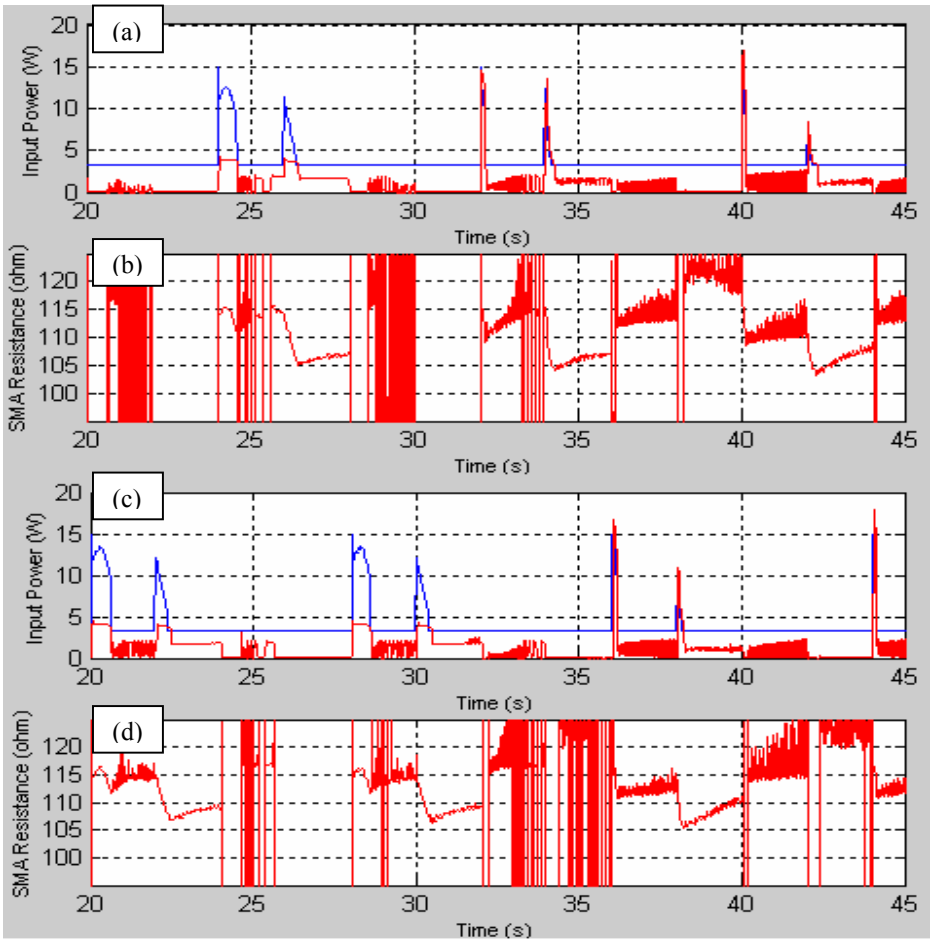

Figure 5.4 Input Power and Resistance Profiles from Fig 5.3: W_{amp} = 15 W; R_{aus} = 105 Ω; Boundary Layer, λ = ±0.5°; Blue Line = Desired Power; Red Line = Actual Power/SMA Resistance; Response of 20-32 s = Power Limiter OFF; Response of 32-45 s = Power Limiter ON. (a) Input Power Profiles for Actuator 1. (b) SMA Resistance Profile for Actuator 1. (c) Input Power Profiles for Actuator 2. (d) SMA Resistance Profile for Actuator 2.

Next, looking at Fig 5.4 (b) and (d) of the SMA resistance profiles, huge fluctuations in the resistance values between 0 Ω and a high resistance value are easily observed. The actuator resistances are measured using relationship between the voltages across the actuators and the currents that flow past them. When the relay controller switches between the two actuators, the current and thus the resistance profile follow the switching of the controller. The result is the recorded fluctuations in the diagrams. Notice also that the profiles of two actuators are out of phase according to the switching nature of the relay controller.

When a dangerously large amount of power is delivered, the resistance of the actuator drops rapidly as it transforms into austenite. According to Equation 5.1, once the SMA resistance approaches the threshold R_{aus}, the mechanism automatically limits the input power to the safe level. This design consideration was successfully implemented in Fig 5.4 (b) and (d). When the resistance value of one actuator reached R_{aus} at 105 Ω, W_{safe} (less than 5 W of input power) was delivered.

There are two factors investigated that can increase the speed of response of the actuators using the power limiter. The first obvious one is the amount of power delivered to the actuators. Another is the duration of exposure to this high input power before the actuators become fully austenitic. This second factor is determined by R_{aus}, the austenite resistance threshold, set in the Simulink control system model.

The effects of varying the level of input power W_{amp} and the threshold R_{aus} on the reduction of rise and fall times of the step response are next to be examined. Fig 5.5 presents responses to step inputs of magnitude ±30°. Results of Fig 5.5 clearly indicate that these factors influence the speed of actuator response. The rise times using different W_{amp} and R_{aus} in the control system are recorded in Table 5.1.

Step Response of Power Limiter Control System with Different Parameters	Recorded Rise Time
W_{amp} = 15 W, R_{aus} = 110 Ω, Desired Step ±30°	0.23 s
W_{amp} = 20 W, R_{aus} = 110 Ω., Desired Step ±30°	0.20 s
W_{amp} = 20 W, R_{aus} = 108 Ω., Desired Step ±30°	0.14 s

Table 5.1 Comparison of Performance using Different Parameters of Power Limiter Mechanism.

Compared to the average rise and fall time of 0.35 seconds of the two-level relay controller response to a similar step input in Chapter 4 Section 4.3.1, the response rise time using 15 W as maximum input power was 0.23 seconds as shown in Fig 5.5 (a) and (b). Using the power limiter mechanism, the control system allowed 15 W of W_{amp} into the plant for very short durations according to the SMA wire resistance measured. The threshold R_{aus} was 110 Ω.

Fig 5.5 (c) and (d) presents the step response using a higher input power, W_{amp} of 20 W. The rise time had been reduced to 0.20 seconds. This was because the increased speed of temperature change in the actuator due to higher input power caused it to contract faster.

Response of Fig 5.5 (e) used the same input power, W_{amp} of 20 W but at a lower R_{aus} threshold of 108 Ω. The effect of this is a 0.06 s reduction to 0.14 seconds in rise time shown in Fig 5.5 (f). The lower threshold allowed higher power input for a longer duration.

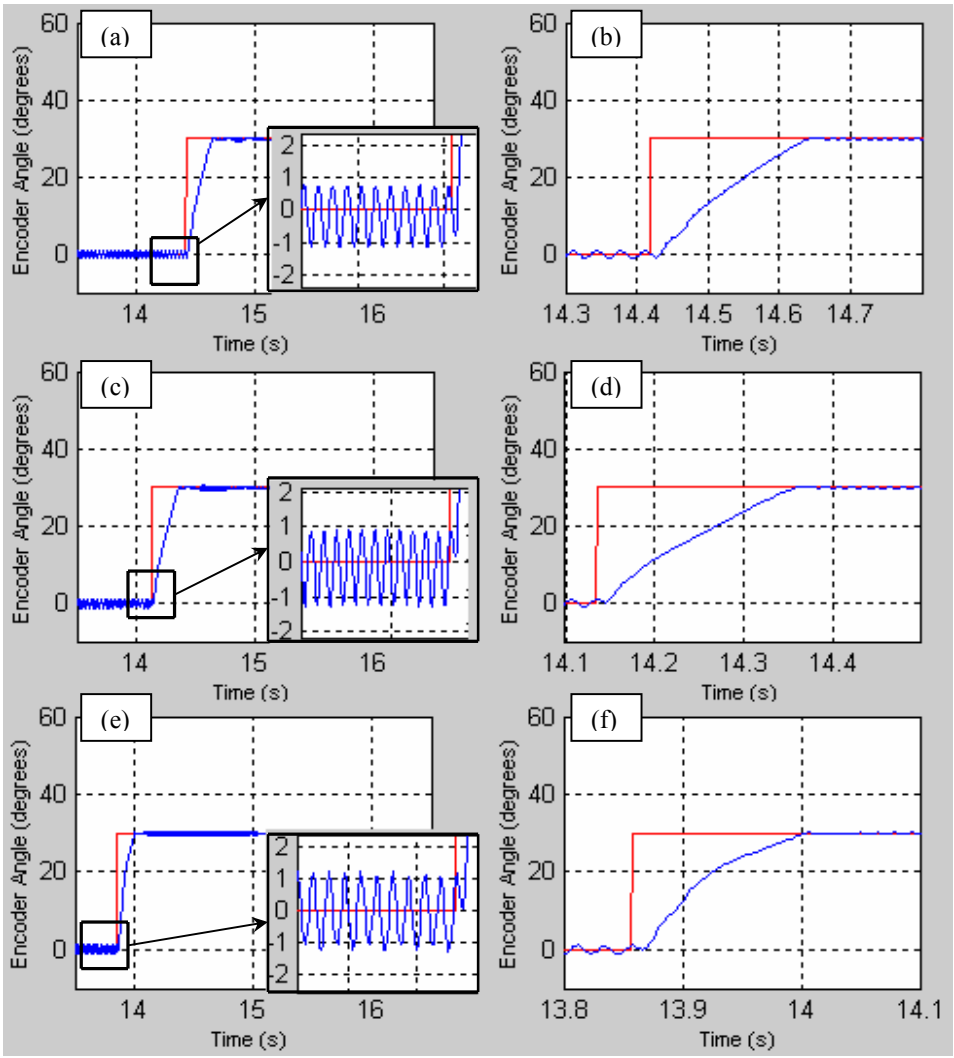

Figure 5.5 Closed Loop Position Step Response Using Control System with Power Limiter Mechanism for a pair of SMA Antagonistic Actuators (No Load Case): Boundary Layer, λ = ±0.5°; Blue Line = Desired Angle; Red Line = Actual Angle.
(a) W_{amp} = 15 W, R_{aus} = 110 Ω, Desired Step ±30° with Close Up View of Limit Cycle.
(b) Detailed Response from (a).
(c) W_{amp} = 20 W, R_{aus} = 110 Ω., Desired Step ±30° with Close Up View of Limit Cycle.
(d) Detailed Response from (c).
(e) W_{amp} = 20 W, R_{aus} = 108 Ω., Desired Step ±30° with Close Up View of Limit Cycle.
(f) Detailed Response from (e).

Larger limit cycle magnitudes of approximately 2° were observed in the close-up views of Fig 5.5. One method to reduce the limit cycle in the 'no load' case is to increase λ, the boundary layer of the relay control. The advantage of this is smaller steady state error and stability. A wider boundary layer causes the power limiter to switch off further from the setpoint and only I_L is delivered. Therefore, the actuator loses its momentum earlier and the result is reduction of limit cycle as shown in Fig 5.6.

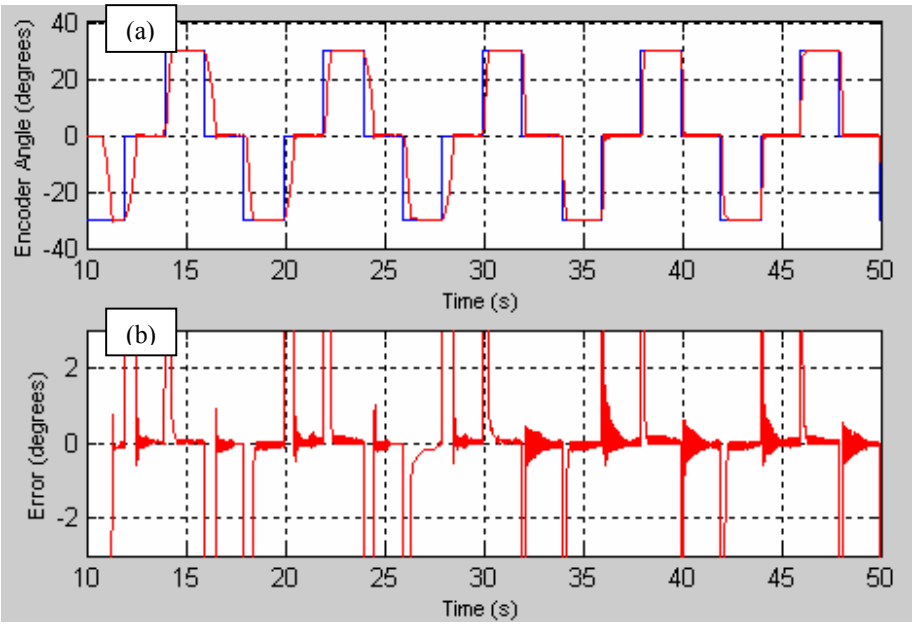

Figure 5.6 Reduced Limit Cycle of Response of the Relay Controller with Power Limiter Mechanism (No Load Case): Boundary Layer, λ = ±1.0°; Blue Line = Desired Angle; Red Line = Actual Angle; Response of 10-30 s = Power Limiter OFF; Response of 30-50 s = Power Limiter ON. (a) W_{amp} = 15 W; R_{aus} = 105 Ω; Desired Step of ±30°. (b) Angle Error from Response (a).

Using λ of ±1.0°, Fig 5.6 (b) indicates that the steady state error converged to the setpoint even with the larger initial error due to the power limiter. In fact, the limit cycle had been decreased to a low magnitude similar to the response with only the two-level relay controller.

The speed of response is also compromised with a wider boundary layer but this will be solved with the implementation of the power limiter. The drawback of this method is that it has no effect with additional loads in the system, as we shall see in Section 5.3.

5.2.2 Tracking Response of Control System With Power Limiter.

Tracking responses to sine inputs with 45° amplitude are presented in Fig 5.7. Similar to the tracking responses of the two-level relay controller, at low frequencies of 0.20 Hz, 0.25 Hz and 0.33 Hz, the power limiter control system tracked the sinusoidal input accurately. Instead of significant lagging behind at 0.5 Hz, the control system managed to perform better than the two-level relay controller did.

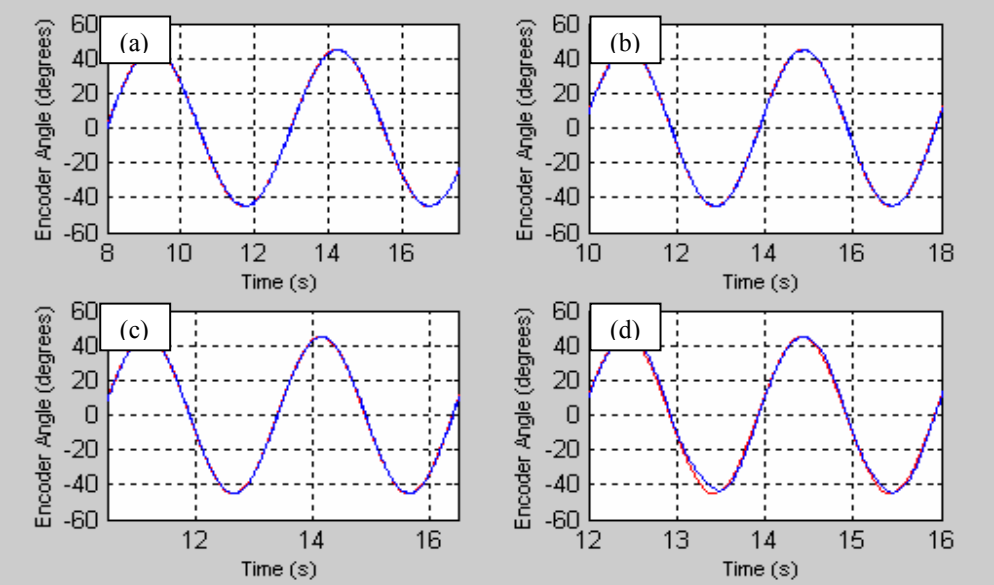

Figure 5.7 Close Loop Position Sine Response (Asin(2πft)) Using Control System with Power Limiter Mechanism for a pair of SMA Antagonistic Actuators (No Load Case): W_{amp} = 15 W; Amplitude = 45°; Blue Line = Desired Angle; Red Line = Actual Angle. (a) Sine Response with f = 0.20 Hz. (b) Sine Response with f = 0.25 Hz. (c) Sine Response with f = 0.33 Hz. (d) Sine Response with f = 0.50 Hz.

The tracking errors of the above response are shown in Fig 5.8. Results are similar to the previous controller where the error revolved about the ±0.5° boundary layer with peak errors occurring at the zero-position. At 0.5 Hz, the error had been significantly reduced (Fig 5.8 (d)) compared to Fig 4.4 (d) of the two-level relay controller.

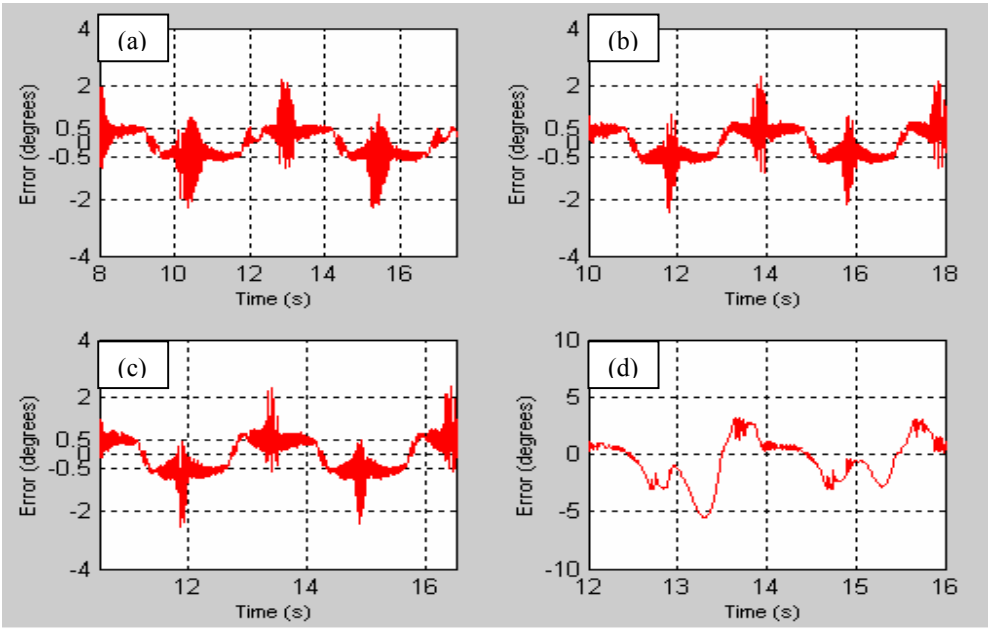

Figure 5.8 Tracking Error for Sine Responses (Asin(2πft)) from Fig 5.7. (a) f = 0.2Hz (b) f = 0.25 Hz. (c) f = 0.33 Hz. (d) f = 0.5 Hz

Direct comparison can be made between the responses of Grant's control system and the improved control system by switching on the power limiter mechanism. Fig 5.9 presents this implementation.

With a frequency of 0.5 Hz of 30° amplitude (Fig 5.9 (a), (c) and (e)), both controllers tracked accurately. However, at a higher frequency of 1 Hz, improvements were observed in Fig 5.9 (b) when the power limiter was switched on at the 30th second.

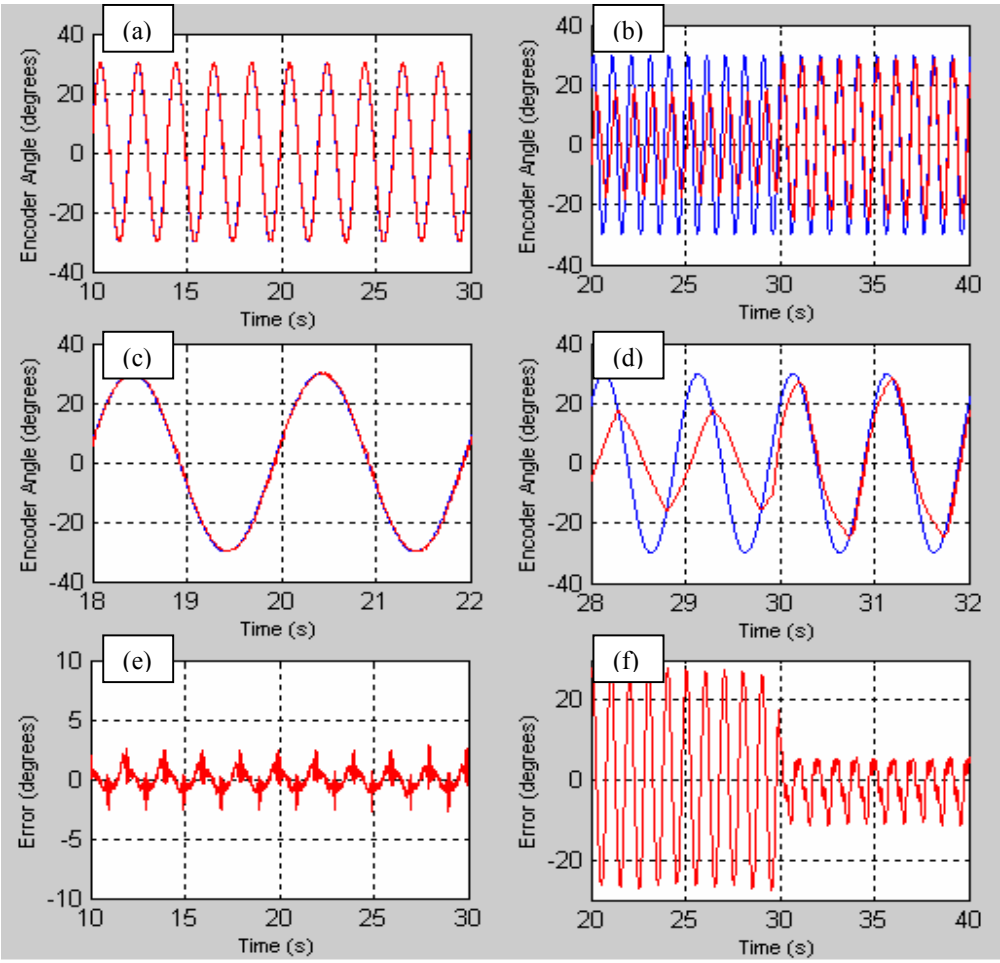

Figure 5.9 Comparison of Tracking Responses between Grant's Two-Level Relay Controller and the Relay Controller with Power Limiter Mechanism (No Load Case): W_{amp} = 20 W; R_{aus} = 105 Ω; Boundary Layer, λ = 0.5°; Amplitude = 30°; Blue Line = Desired Angle; Red Line = Actual Angle; Response of 10-20s = Power Limiter OFF; Response of 20-30s = Power Limiter ON.
(a) Sine Response of f = 0.50 Hz (Power Limiter ON from 20th Second)
(b) Sine Response of f = 1.00 Hz (Power Limiter ON from 30th Second)
(c) Detailed Response from (a). (d) Detailed Response from (b).
(e) Tracking Error of Response (a). (f) Tracking Error of Response (b).

The power and resistance profiles of experimental results in Fig 5.9 (b) are presented in Fig 5.10. Again, before switching on the power limiter, safe power levels of less than 5 W was delivered to the actuators causing a slow response as observed between the 20th to the 30th second of the response in Fig 5.9 (b). Once switched on, the tracking error in Fig 5.9 (d) had been reduced drastically.

Although the desired input power, W_{amp} had been set at 20 W, the control system did not deliver that amount of power as shown in Fig 5.10. This is because of the design requirements summarised in Equation 5.1. According to the equation, the maximum input power will not be delivered if the actuator resistance is less than R_{mar}. Continuous tracking had kept the actuators at high temperatures and at resistance values lower than R_{mar}.

This is an indication that for high-speed continuous tracking, the power limiter mechanism does not require extremely high power inputs, as they are unnecessary.

The switching of the actuators due to the relay control is clearly observed in Fig 5.10 (b) and (d) as the resistance values fluctuated from 0 Ω to a high value periodically. The profiles also clearly show the drop in resistance values as the actuators were heated and transformed to the austenitic phase. Note the power limiting effect as the threshold R_{aus} of 105 Ω was reached.

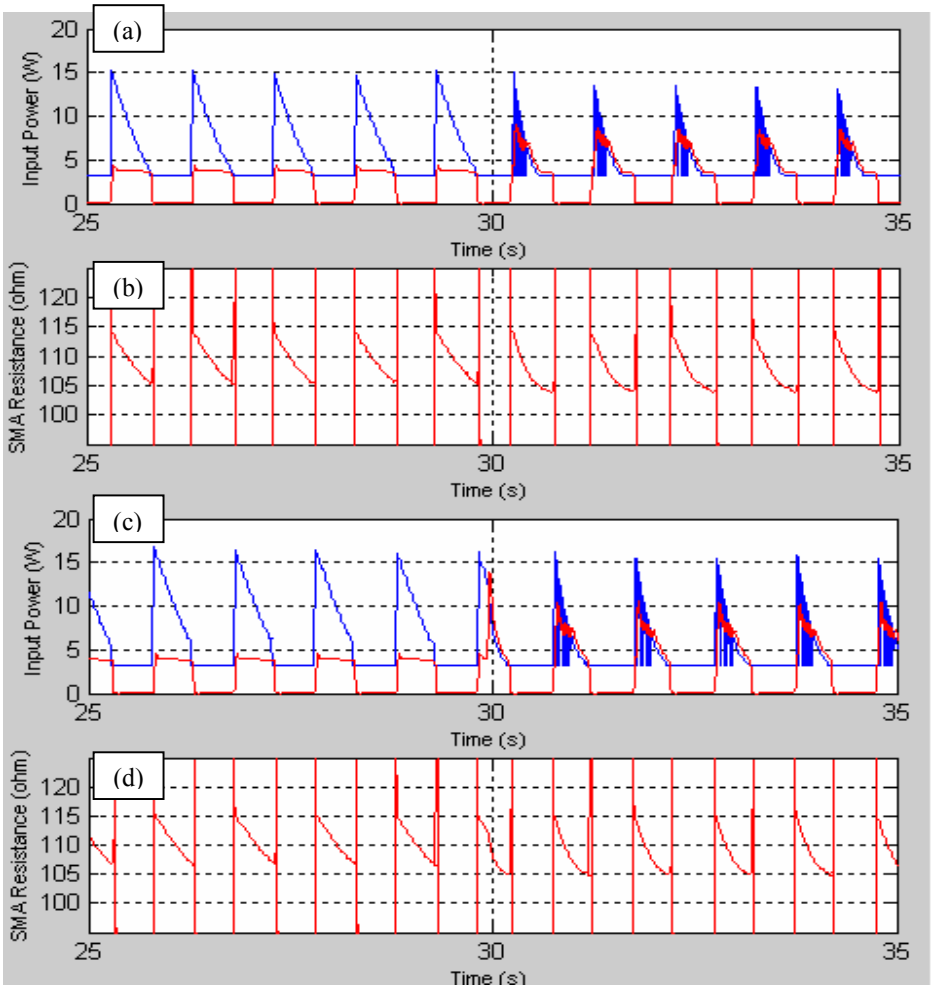

Figure 5.10 Input Power and Resistance Profiles from Fig 5.9(b). W_{amp} = 20 W; R_{aus} = 105 Ω; Boundary Layer, λ = ±0.5°; Blue Line = Desired Power; Red Line = Actual Power/SMA Resistance; Response of 25-30 s = Power Limiter OFF; Response of 30-35 s = Power Limiter ON (a) Input Power Profiles for Actuator 1. (b) SMA Resistance Profile for Actuator 1.(c) Input Power Profiles for Actuator 2. (d) SMA Resistance Profile for Actuator 2.

5.3 Position Control – With a Load

The following figures show the effects of adding a copper rod to the actuator system.

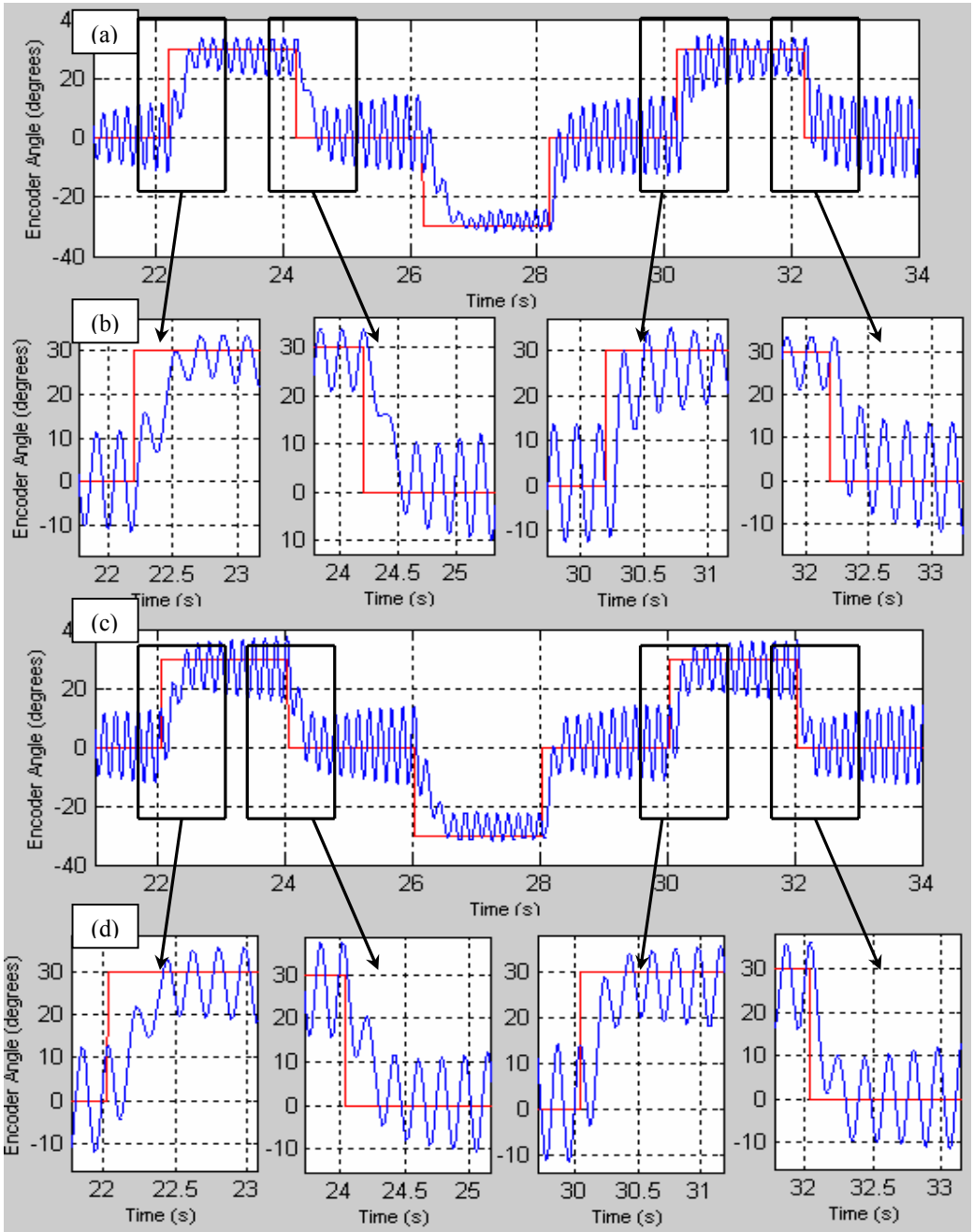

Figure 5.11 *Close Loop Position Step Response Using Controller with Power Limiter Mechanism for a pair of SMA Antagonistic Actuators (With Load Case): Blue Line = Desired Angle; Red Line = Actual Angle. Response of 21-28 s = Power Limiter OFF; Response of 28-34 s = Power Limiter ON.*
(a) W_{amp} = 10 W, R_{aus} = 108 Ω, Desired Step ±30°. (b) Detailed Views from (a).
(c) W_{amp} = 15 W, R_{aus} = 108 Ω, Desired Step ±30°. (d) Detailed Views from (b).

It is clearly shown in Fig 5.11 that the power limiter had no effect in the reduction of the magnitude of the limit cycle when an additional load was introduced. . The limit cycle does not converge within the boundary layer due to the increased momentum of the system.

Figures 5.11 (a) and (c) present responses where the power limiter was only switched on from the 28^{th} second. Tests had been carried out to examine the effects of increasing the width of the boundary layer but no improvements had been made. The larger momentum of the system with the additional 40 g load could not be diverted or reduced.

In fact, the experiments conducted seem to suggest that there is a slow degradation of performance in terms of limit cycle when the power limiter is on. The additional inertia in the system may have overworked the actuators and caused the actuators to stretch beyond their strain. It is also possible that the wire actuators were becoming overheated and damaged after long duration of extreme current inputs.

However, the graphs Fig 5.11 (b) and (d) clearly indicate that the rise and fall times of responses to a step input had improved with the mechanism even with the additional load in the plant.

With only the safe I_H level of the relay controller, the actuators did not have sufficient force to fully overcome the oscillations of the copper rod and contract to the required setpoint. A direct step to the setpoint did not occur but instead, oscillations caused an opposite motion of the actuators. This was observed in the close-up views of Fig 5.11 (b) and (d) before the power limiter was switched on.

Once the power limiter was implemented, the actuators had enough input current to overcome the momentum of the rod and almost instantaneously reach the setpoint.

5.4 Chapter Summary

5.4.1 Evaluation of Performance.

It was shown that with the power limiter, the speed of response of the SMA actuators had been significantly improved compared to Grant's two-level relay controller.

For the 'no load' case, the rise time of the step response had been reduced to a low of 0.14 seconds by varying parameters such as maximum input power and R_{aus}. Note that the experimental set-up is capable of delivering higher power inputs than 20 W so the potential of this design is not limited to the response speed recorded in this work. The control system also managed to track a 30° sinusoidal input at 0.5 Hz and 1 Hz better than the relay controller.

However, the power limiter mechanism is also not free from disadvantages. One of them is the large magnitude limit cycles observed in step responses with the additional load in the system. In spite of that, the control system has great potential to achieve fast as well as accurate response from SMA actuators with further improvements.

5.4.2 Comparison of Results from Both Control Systems.

A brief overall comparison of both controllers in Chapter 4 and Chapter 5 will be presented.

For both the 'no load' and 'with load' cases, the control system with the power limiter mechanism was found to have a significantly faster response compared to Grant's two-level relay controller.

However, the performances of both controllers degrade drastically when an additional load is present in the system. The result is drastic increase in the limit cycle magnitude and the average steady state error. The power limiter mechanism does not appear to have any influence on the improvement of the limit cycle. A possible modification to improve the performance is to increase the boundary layer but this results in slower response, as the I_L pulse will be activated for a longer time.

The increase in the limit cycle magnitude caused by the external load represents one of the major drawbacks of the two-level relay controller, regardless of whether the power limiter mechanism has been implemented. This is often undesirable in robotics applications as limit cycles cause excessive wear of mechanical components. It was observed that the large limit cycles were symptoms that the controller was switching between the actuators repeatedly and excessively. The possible implications to the SMA wires are fatigue and reduction of life cycle.

Chapter 6: Conclusion

In this chapter, the outcomes of the project are stated and an appraisal of the overall successfulness of the project is given. Further logical developments for the project are also suggested.

6.1 Summary

The outcome of the project was the successful design and fabrication of a complete hardware and software system that meets the objective set for this engineering project. An improved control system had been employed to demonstrate that the speed of Shape Memory Alloy actuator wires can be further increased compared to a control system implementing only a two-level relay controller.

The advantages of relay control are its easy implementation and combined with an antagonistic arrangement of actuators, the simplification of the control design. Grant's two-level relay controller also has the advantage of smoother and more stable response.

The improved control system has a power limiter mechanism in addition to the two-level relay controller. Therefore, it not only reaps the benefits of the relay controller, but also utilises the advantage of the higher input power without damaging the actuators. The result is faster responses compared to Grant's control system. Its current weaknesses include large magnitude limit cycles at the steady state.

However, it is felt that the amount of achievements made in this project are very substantial. Not only were design and experimentation of the control systems carried out, the project involved a significant effort of fabricating the entire experimental set-up and testing both of its hardware and software components.

The current experimental set-up exhibits potential improvements and operability. It is highly anticipated by both the student and the supervisor involved in this project that very fast and accurate motion control of SMA actuator wires could be achieved with more time and development.

It is also felt that only time limitations and unprecedented experimental complications that prevented further improvements in the control system as well as the development of the pantograph robotic device. The door for future work with this project and its experimental set-up has been opened.

6.2 Future Work

This section will discuss some future improvements and research directions with respect to both the hardware and software components of this project.

Although very fast actuation had been achieved for the SMA actuators, the accuracy of the control system has been a problem. The power limiter mechanism exhibited great potential but the control system may be improved by introducing a damping mechanism around the region close to the setpoint to reduce the effects of limit cycles at steady state.

The concept is to reduce the momentum of the system by allowing the system to switch from the high current pulse to the I_L pulse or zero and then apply an I_L pulse in the other antagonistic actuator. This applies a force in the opposite direction attempting to damp the momentum of the system. This mechanism is dependent on the velocity of the actuators. When the velocity is above a certain threshold, the damping mechanism kicks in and begins to reduce the limit cycle magnitude to an acceptable level. The influence of additional inertia to the system needs to be considered especially for the successful control of the two degree-of-freedom pantograph device.

The next logical step after successfully implementing a control system that eliminates the limit cycle is to develop the pantograph control system. A functioning pantograph control system that controls both antagonistic actuator pairs had been developed. It managed to track a square motion at 1 Hz using the pantograph but lacks accuracy. This bears research and development.

A few structural elements also warrant further development:

- The current experiment rig requires improvising especially in terms of slack and possible entanglement of the actuator wires.
- Load cells can be added to the experiment rig to measure the force of the SMA actuators to provide complete information regarding the state of the actuators.
- The current actuator system is a type of mass-spring system with no damping mechanism. It is therefore highly possible to incorporate magnetic damping into the system to make it into a mass-spring-damping system. This is to reduce the limit cycle.
- The pantograph device bears redesigning due to slack and twisting of the device during actuation. Better hinges may need to be considered.

References

[1] Brailovski, V., Trochu, F., Daigneault, G. (1996) Temporal Characteristics of Shape Memory Linear Actuators and Application to Circtui Breakers. *Materials & Design.* 17, 3:151-158.

[2] dSPACE (2002). DS1104 R&D Controller Board Installation and Configuration Guide For Release 3.4.

[3] dSPACE (2002). ControlDesk Experiment Guide For Release 3.4.

[4] Dynalloy, Inc. Flexinol.
http://www.dynalloy.com/
Last updated February 2003
[Accessed 18 May 2003]

[5] Hodgson, D., Wu M. (1999) Shape Memory Alloys. Shape Memory Applications Incorporated. California.
http://www.sma-inc.com/SMAPaper.html
[Accessed 14 September 2002]

[6] Grant, D. (1999) Accurate and Rapid Control of Shape Memory Alloy Actuators. Doctor of Philosophy Thesis. McGill University.

[7] Gorbet, R. (1996) A Study of the Stability and Design of Shape Memory Alloy Actuators. Master of Applied Science Thesis. University of Waterloo.

[8] Halliday, D., Resnick, R., Walker, J. (1993) Fundamentals of Physics Extended. 4th Edition. USA: Wiley.

[9] Kotil, T., Sehitoglu, H., Chumlyakov Y. Resistance Behavior of Transforming Material. Mechanical and Industrial Engineering Dept. University of Illinois.

[10] Mihalcz, I. (2001) Fundamental Characteristics and Design Method for Nickel-Titanium Shape Memory Alloy. *Periodica Polytechnica Ser. Mech. Eng.* 45, 1:75-86.

[11] Mosley, M.,Mavroidis, C., Pfeiffer, C. Design and Dynamics of A Shape Memory Alloy Wire Bundle Actuator. Department of Mechanical and Aerospace Engineering. The Stage University of New Jersey.

[12] Rediniotis, O., Lagoudas, D. Shape Memory Alloy Actuators As Locomotor Muscles. Aerospace Engineering Department. Texas A&M University.

[13] Serneels, A. Shape Memory Alloy Characterisation and Optimization. AMT @ Medical Technologies, Belgium.

[14] Shape Memory Applications Incorporated. California. Selected Properties of NiTi
http://www.sma-inc.com/NiTiProperties.html
[Accessed 14 September 2002]

[15] Shape Memory Applications Incorporated. California. NiTi Actuator Wire Properties.
http://www.sma-inc.com/Actuators.html
[Accessed 14 September 2002]

[16] US Digital. Vancouver. HEDS Optical Encoder Module.
http://www.usdigital.com/products/heds
Last updated 5 May 2003 [Accessed 22 May 2003]

Appendix A: Properties of NiTi and Flexinol[tm]

Flexinol[tm] is the trade name of the NiTi shape memory alloy specifically manufactured and marketed by Dynalloy Inc. The following table of properties for Flexinol[tm] actuator wires is obtained from [**15**].

Table A.1 Properties of Flexinol[tm] Actuator Wires.

Wire Diameter	Resistance (Ohms/ Inch)	Maximum Pull Force	Approximate* Current at Room Temperature	Contraction as a Percent of Length	Contraction Time * at 21 deg.C	Off Time for 70 C Wire	Off Time for 90 C Wire
0.001"	45.0	7 grams	20 mA	4%	1 sec.	0.1 sec.	0.06 sec.
0.0015"	21.0	17 grams	30 mA	4%	1 sec.	0.25 sec.	0.09 sec.
0.002"	12.0	35 grams	50 mA	4%	1 sec.	0.3 sec.	0.1 sec.
0.003"	5.0	80 grams	100 mA	4%	1 sec.	0.5 sec.	0.2 sec.
0.004"	3.0	150 grams	180 mA	4%	1 sec.	0.8 sec.	0.4 sec.
0.005"	1.8	230 grams	250 mA	4%	1 sec.	1.6 sec.	0.9 sec.
0.006"	1.3	330 grams	400 mA	4%	1 sec.	2.0 sec.	1.2 sec.
0.008"	0.8	590 grams	610 mA	4%	1 sec.	3.5 sec.	2.2 sec.
0.010"	0.5	930 grams	1000 mA	4%	1 sec.	5.5 sec.	3.5 sec.
0.012"	0.33	1250 grams	1750 mA	4%	1 sec.	8.0 sec.	6.0 sec.
0.015"	0.2	2000 grams	2750 mA	4%	1 sec.	13.0 sec.	10.0 sec.

* The contraction time is directly related to current input. The figures used here are only approximate since room temperatures, air currents, and heat sinking of specific devices vary. Currents which take one second to heat the wire can be left on without overheating it.

The following Table A.2 of NiTi Properties is taken from [**14**].

Table A.2 Selected Properties of NiTi

Transformation Properties	
Transformation Temperature	-200 to 110 deg. C
Latent Heat of Transformation	5.78 cal/g
Transformation Strain	
For a single cycle	max 8 %
For 100 cycles	6 %
For 100,000 cycles	4 %
Hysteresis	30 to 50 deg. C
Physical Properties	
Melting Point	1300 deg. C
Density	6.45 g/cm^3
Thermal Conductivity	
Austenite	0.18 W/cm * deg. C
Martensite	0.086 W/cm * deg. C
Coefficient of Thermal Expansion	
Austenite	11.0E-6/deg. C
Martensite	6.6E-6/deg. C
Specific Heat	0.20 cal/g * deg. C
Corrosion Performance	excellent
Electrical and Magnetic Properties	
Resistivity [resistance = resistivity * length / cross-sectional area]	
Austenite	approx. 100 micro-ohms * cm
Martensite	approx. 80 micro-ohms * cm
Magnetic Permeability	< 1.002
Magnetic Susceptibility	3.0E6 emu/g
Mechanical Properties	
Young's Modulus	
Austenite	approx. 83 GPa
Martensite	approx. 28 to 41 GPa
Yield Strength	
Austenite	195 to 690 MPa
Martensite	70 to 140 MPa
Ultimate Tensile Strength	
Fully Annealed	895 MPa
Work Hardened	1900 MPa
Poisson's Ratio	0.33
Elongation at Failure	
Fully Annealed	25 to 50 %
Work Hardened	5 to 10 %

Appendix B: Set-Up and Design Procedures

Appendix B discusses the procedures and principles of the crucial components of the experimental set-up. SMA wire standardisation and hardware testing procedures for the amplifier circuits, experiment rig will be described. The conceptual designs of the Simulink models such as encoder initialisation as well as analog data acquisition and processing are also discussed.

B.1 Flexinol^{tm} Wire Standardisation

Each new Flexinol^{tm} wire of length 1.2 m is cut and allowed to dangle freely. A limiting current of 180 mA is applied through the dangling wire to fully contract the wire. This is the safe current level that takes one second to heat the wire and can be left on without overheating the wire according to [**15**]. Each wire is then stretched using a standard weight of 0.2 kg such that the martensite structure is fully detwinned. This is the maximum length of the wire and it cannot be stretched further without damaging the wire.

When fixing the wire into the rig, the pulley is rotated and fixed at approximately 100° from the neutral position of the pulley. The wire is made taut using a small weight before being clamped to the brackets at the lower part of the experiment rig permanently for electrical connection. The same is repeated for the other wire in antagonistic position. Fig 3.1 presents a graphical representation of this procedure.

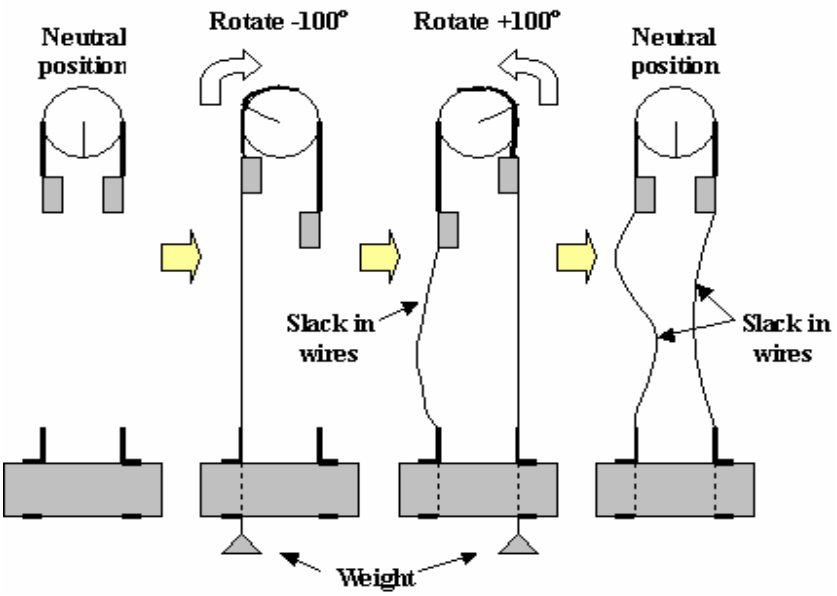

Figure B.1 Procedures for Fixing Flexinol^{tm} Wires into Experiment Rig

The objective of this is to allow the actuators to achieve the maximum rotation of ±100° from the neutral position theoretically. This procedure also ensures the repeatability of experiment. If an actuator wire is damaged during the experiment, a new wire can replace it if all wires go through the same standardisation process.

B.2 Testing of Amplifier Circuits and Electrical Connections

The following procedures were completed first to prevent oversupply of current and thus damage the expensive actuators and Field Effect Transistors:

- Wire up and connect all the components and conduct a continuity test using a multimeter on crucial connections and pins
- Switch on the power supply and check important points on the circuit (especially at inputs, transistor and FET pins) using multimeter to ensure normal functioning.
- Use a low, constant voltage supply instead of the DAC voltage input. Slowly increase the current from 0 A to 180 mA (the safe current level) and observe any changes in the SMA wire connected to the circuit. Check that the SMA wire is contracting as expected. Ensure no short-circuiting along the SMA wire.
- Check that all four amplifiers are functioning properly.

B.3 Optical Encoder Module Initialisation

Initialising the encoder module is important before any implementation could be made to control the actuation of the SMA. The objective is to measure the absolute rotation angle of the encoder disk, and thus the displacement of the wires with respect to a known initial position, which is the position of the Index Pulse on the disk.

The Simulink model (Fig B.2) that implements the initialisation has these features:

- Once started, the model must slowly but increasingly supply current through the amplifier circuit to actuate one Flexinol^{tm} wire until the Index Pulse is detected.
- If no detection is made, the other wire is actuated to rotate the disk in the opposite direction until detection.
- Once the Index Pulse is detected, the position of the encoder is set to zero. This will be referred to as the ‘zero-position’. The initialisation phase is ended at this point and the control phase will commence.
- The encoder records the position of the disk in terms of encoder lines or CPRs (Refer to Section 2.2.5 for definition). The model has a feature to convert encoder line to rotation angles (°) or actual displacement of the wires.

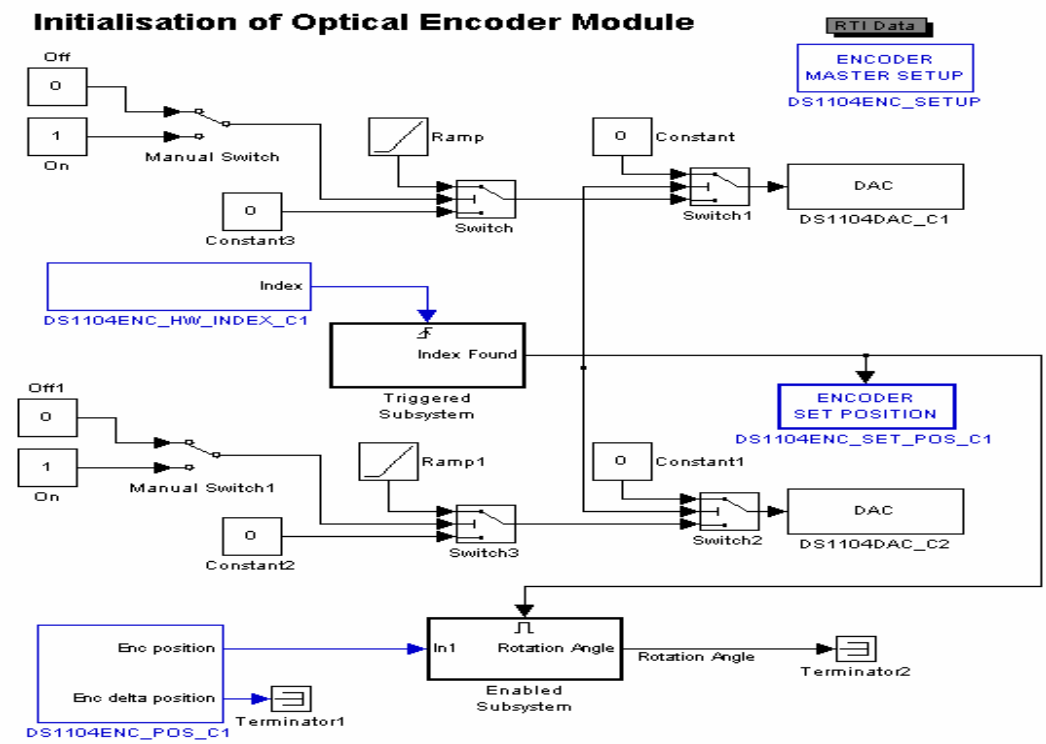

Figure B.2 Simulink Model for Index Pulse Detection and Initialisation

From the Simulink model in Fig B.2, the Index Pulse on the encoder disk is detected using the DS1104_ENC_HW_INDEX_C1 block. The detection produces a rising edge signal and triggers the DS1104ENC_SET_POS_C1 block to set the encoder position counter to '0', or the zero-position. The DS1104_ENC_POS_C1 block reads the position from the channels of the encoder disk. Given in encoder lines, the position of the encoder can be measured as rotation angles once the index detection signal triggers it. This allows the user to measure the rotation angle of the pulley from a known zero-position.

B.4 Analog Data Acquisition and Processing

The amplifier circuit provides measurement of voltages at two points on the circuit. These analog voltage inputs are linked to the 12-bit parallel ADCs and the 16-bit multiplexed ADC. The data can be processed to provide sufficient information regarding the state of the SMA wires. In particular, the electrical resistance and the power input to the SMA wires can be measured using simple circuit laws as described in the following.

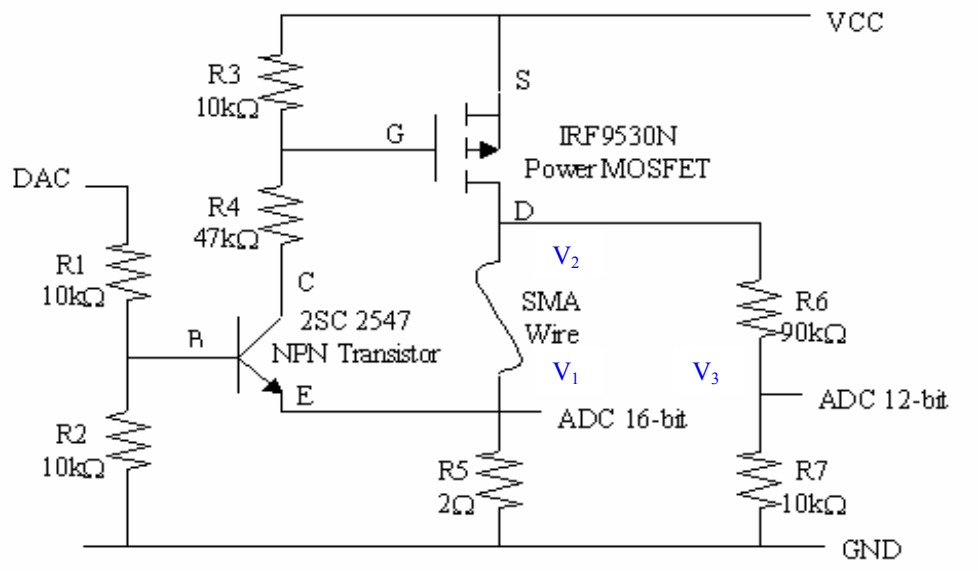

Figure B.3 Current Amplifier Circuit

- V_1 = Voltage measured at ADC 16-bit.
- V_3 = Voltage measured at ADC 12-bit.
- Assuming that Current through SMA ≅ Current through Resistor R5 as Emitter Current is very small, $I_E \cong 0$.
- Therefore,

$$\text{Current through SMA, } I_{SMA} \cong I_{R5} = \frac{V_1}{R5} \quad \text{(B.1)}$$

- Current through Resistor R6, I_{R6} = Current through Resistor R7, I_{R7}
- Therefore,

$$\text{Current through Resistor R6, } I_{R6} = I_{R7} = \frac{V_3}{R7} \quad \text{(B.2)}$$

- Since,

$$V_2 - V_3 = I_{R6} \times R6 \quad \text{(B.3)}$$

- Thereofore,

$$\text{Voltage at MOSFET Drain, } V_2 = I_{R6} \times R6 + V_3 \quad \text{(B.4)}$$

- Hence,

$$\text{SMA Wire Resistance, } R = \frac{V_2 - V_1}{I_{SMA}} \quad \text{(B.5)}$$

- Hence,

$$\text{SMA Input Power, } P = I_{SMA}^2 \times R \quad \text{(B.6)}$$

Using the above circuit relationships, a Simulink model had been designed for analog data acquisition and processing as shown in Fig B.4.

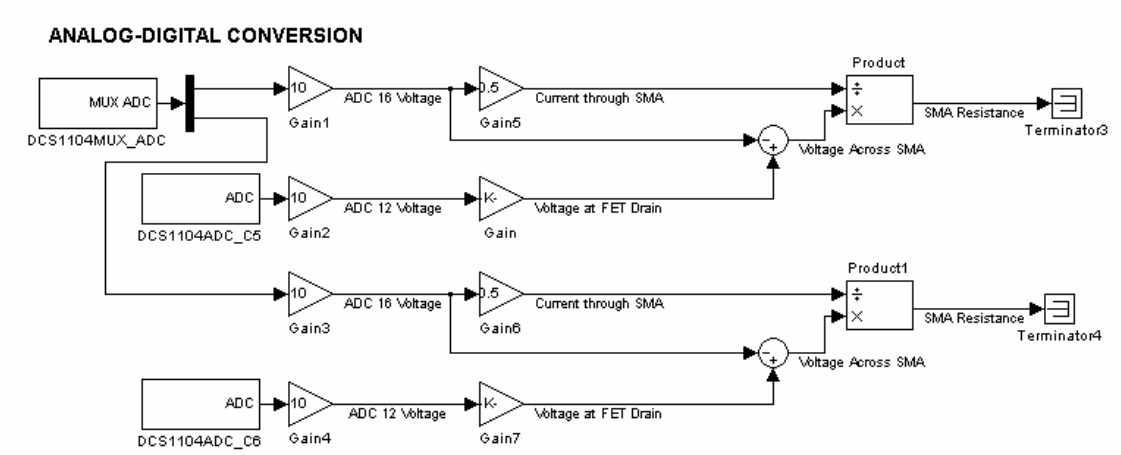

Figure B.4 Simulink Model for Analog-To-Digital Conversion and Data Processing

Appendix C: Simulink Models

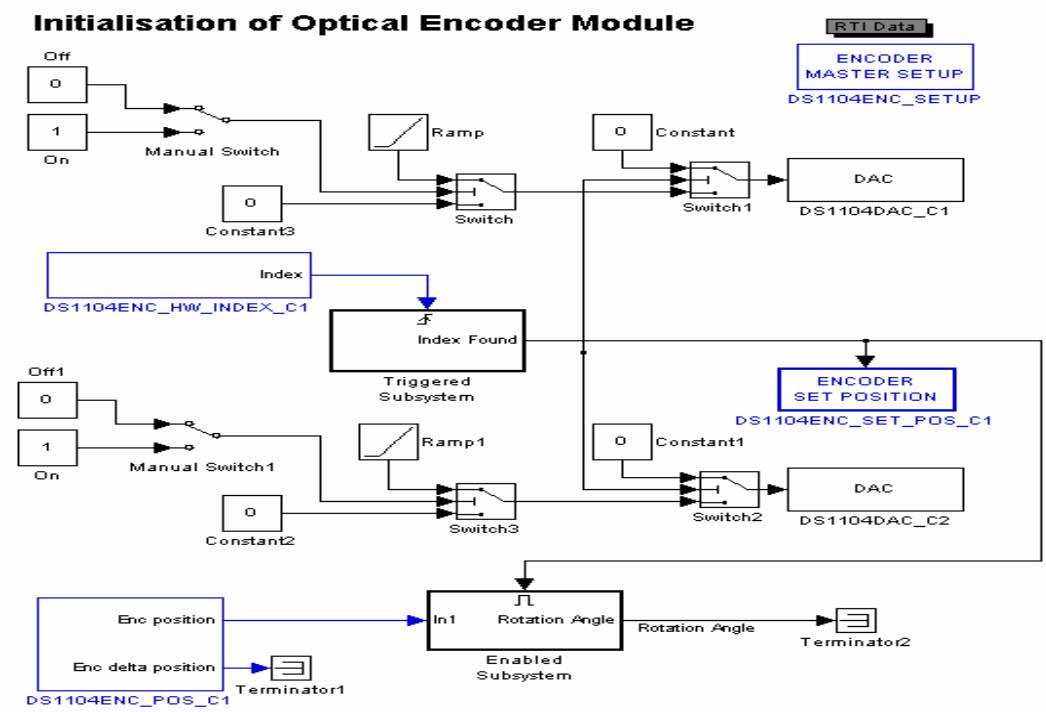

Figure C.1 Initialisation of an Optical Encoder Module

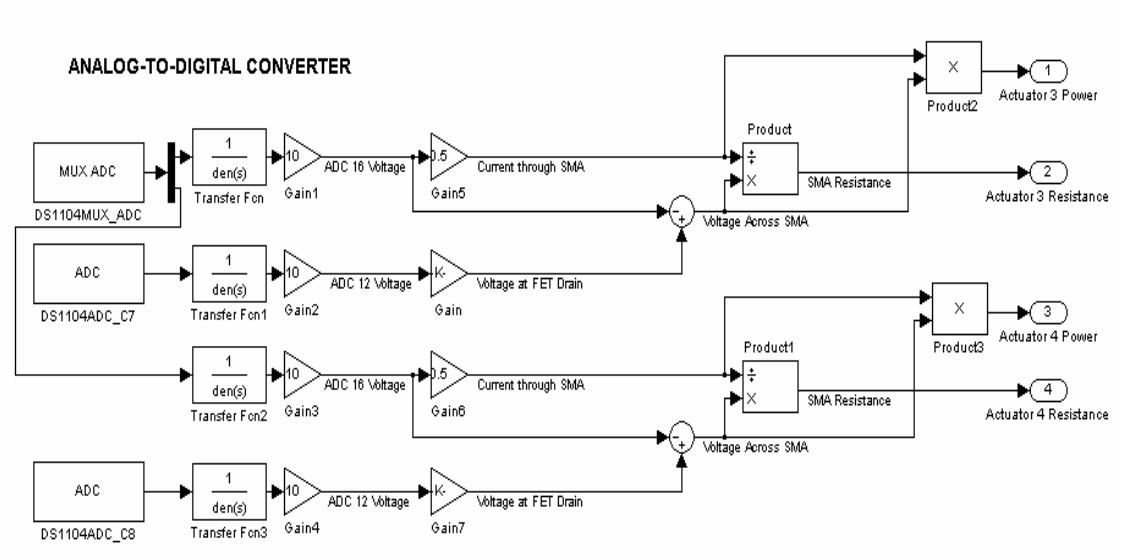

Figure C.2 Analog-Digital Conversion and Data Processing with Software Filtering

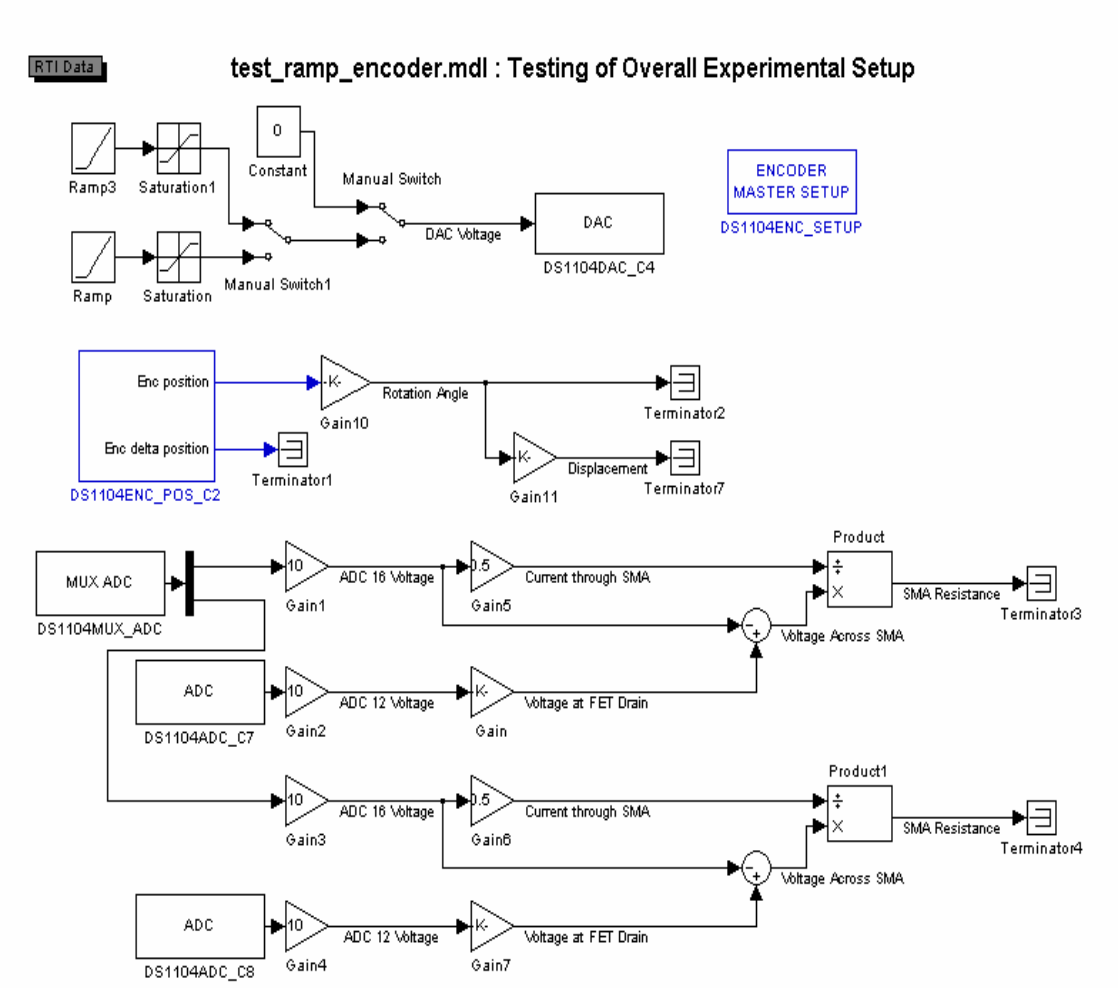

Figure C.3 Open Loop Simulink Model for Experimental Setup Testing

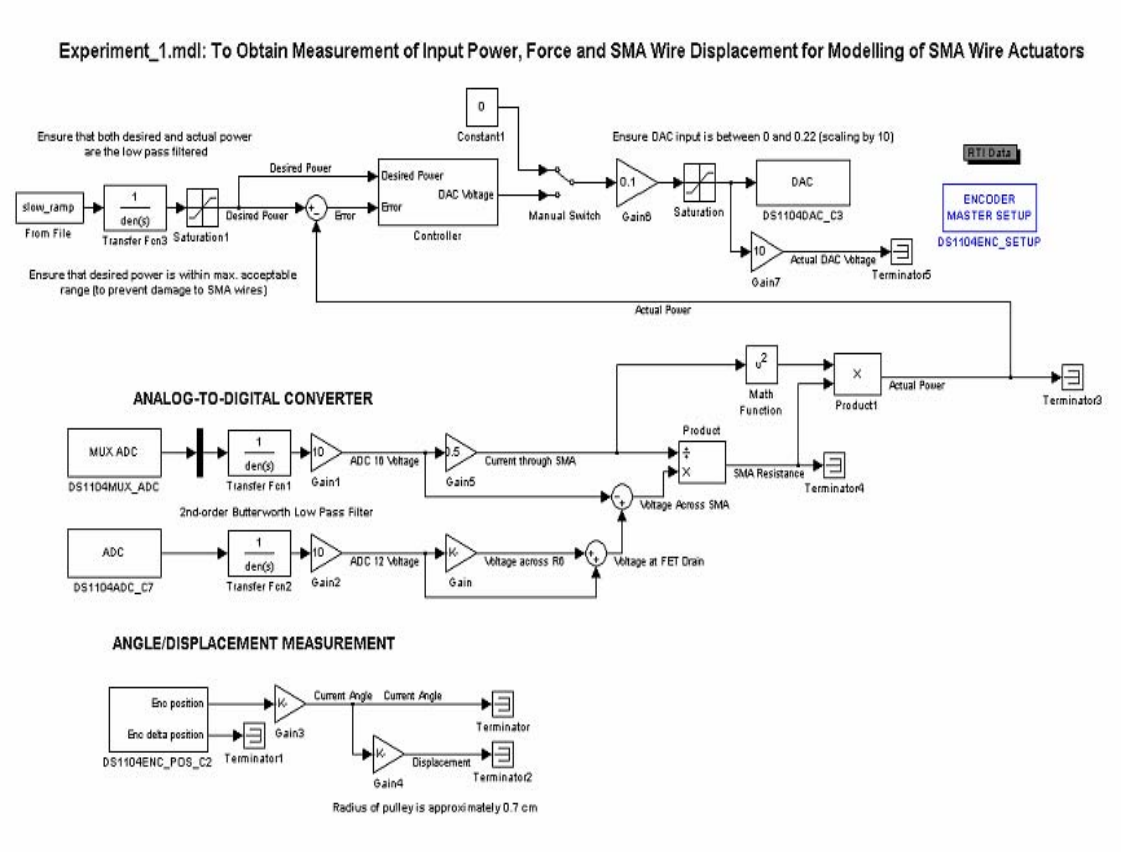

Figure C.4 Closed Loop Modelling Experiment Model

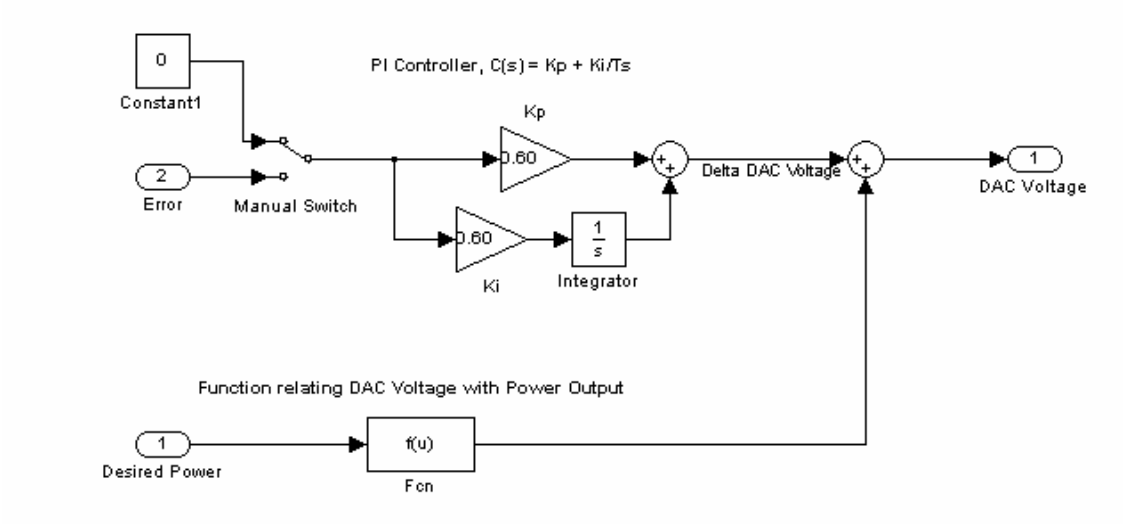

Figure C.5 Proportional-Integral Controller for Modelling Experiment

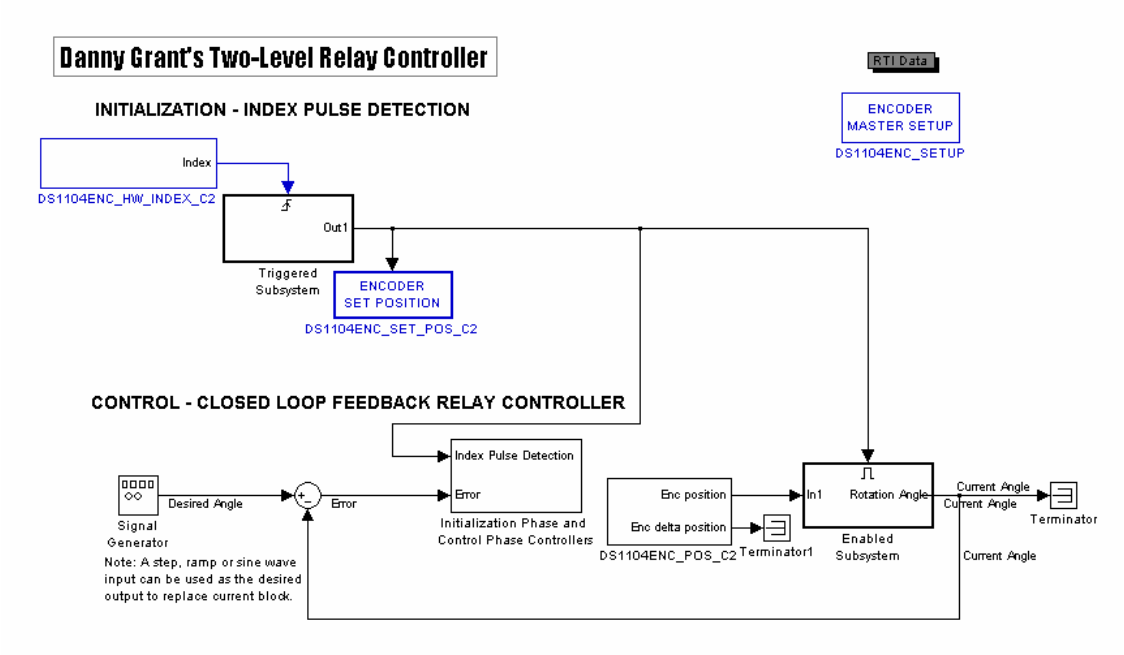

Figure C.6 Closed Loop Position Model with Relay Controller

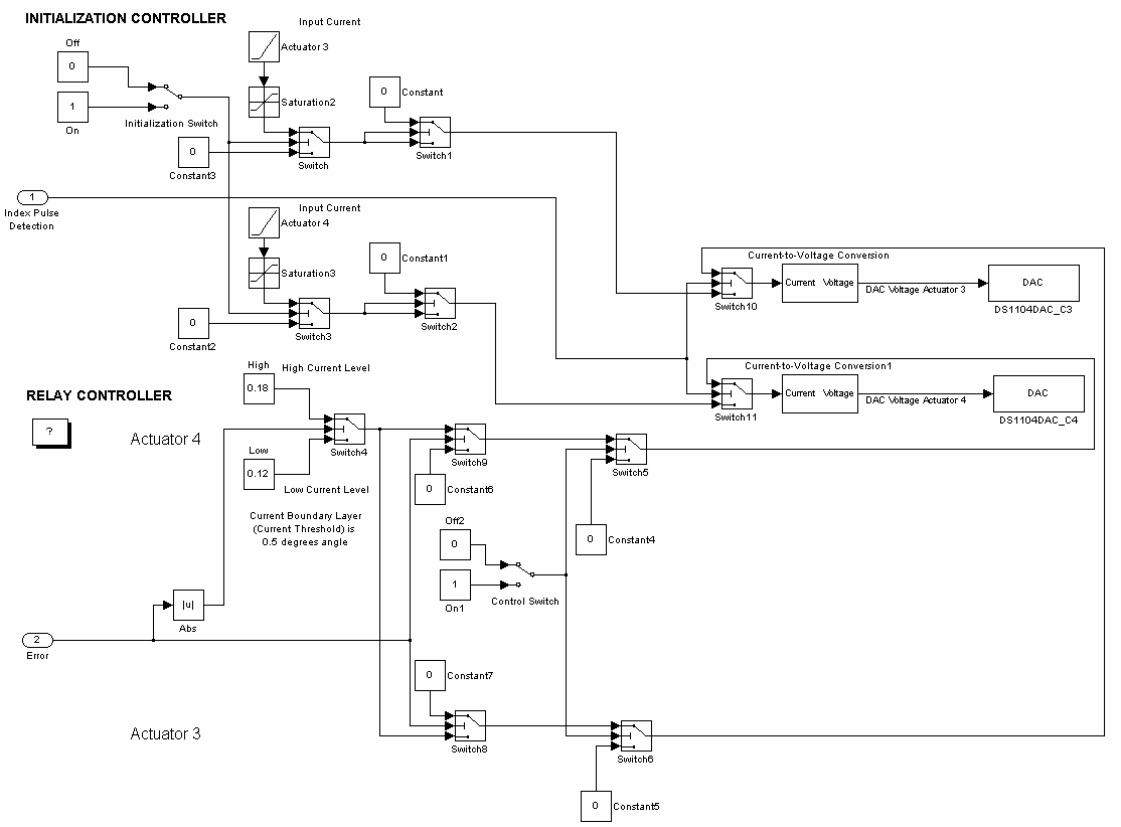

Figure C.7 Initialisation and Relay Controller

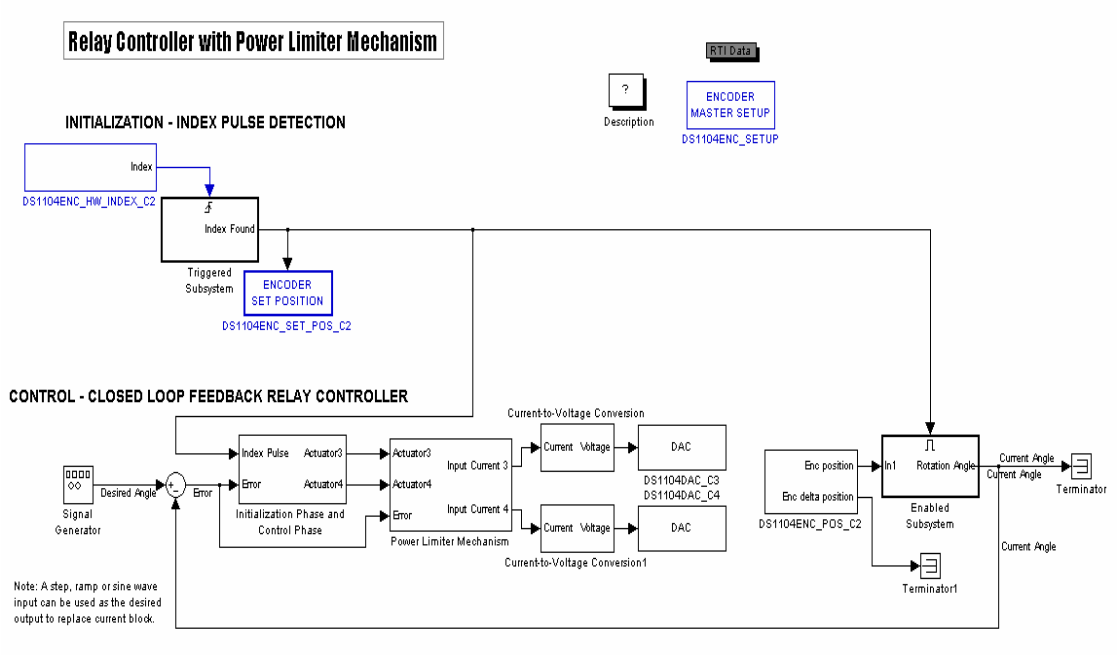

Figure C.8 Closed Loop Position Control with Power Limiter Mechanism

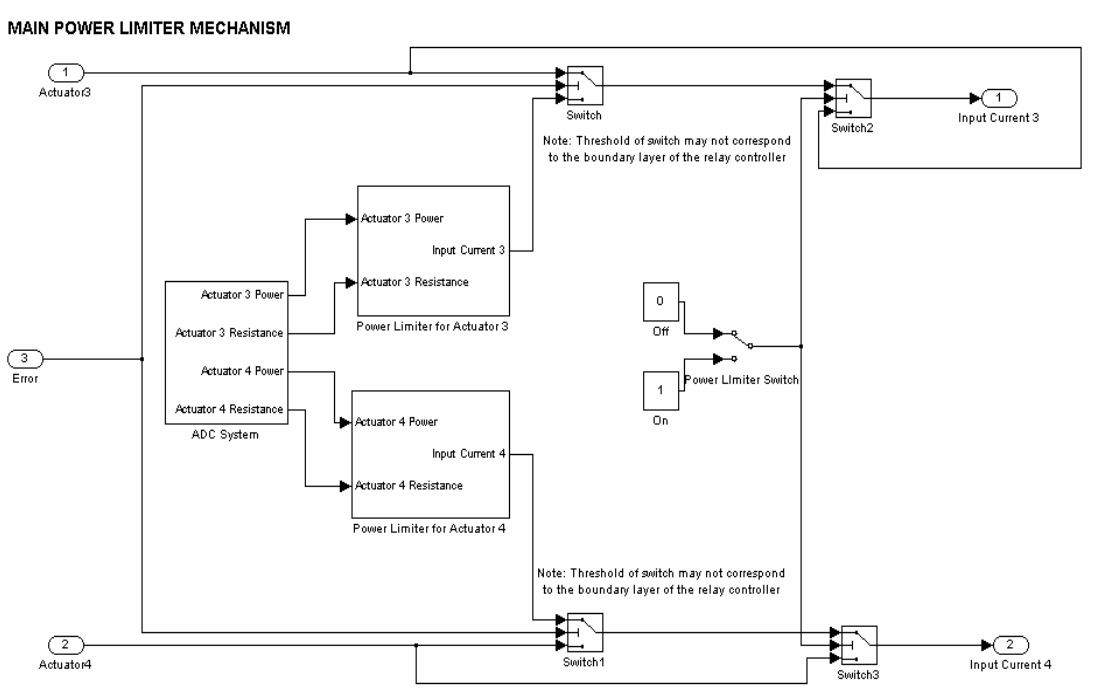

Figure C.9 Main Power Limiter Mechanism

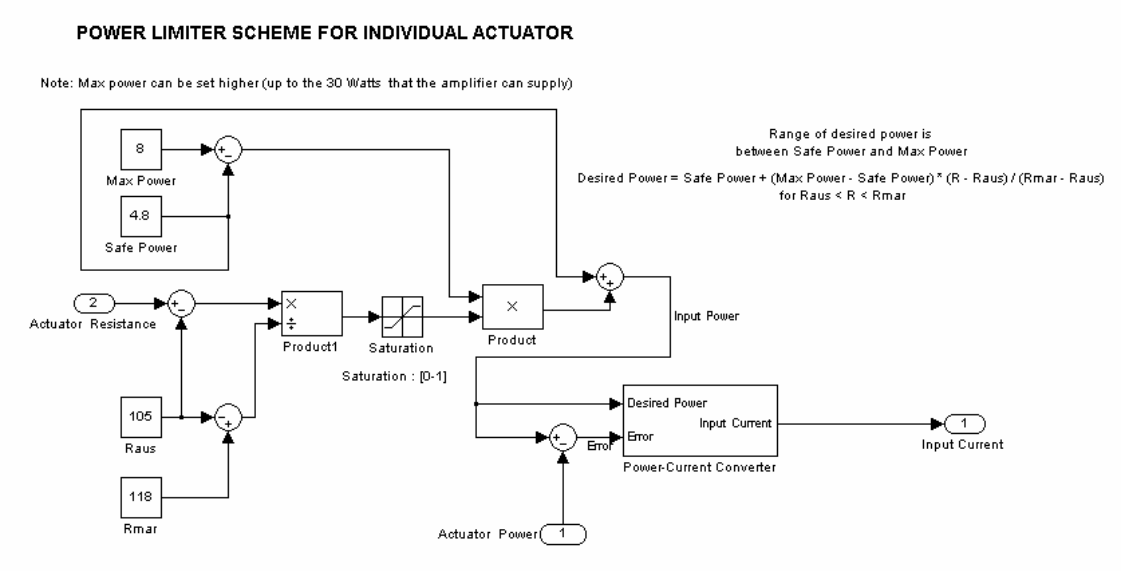

Figure C.10 Power Limiter Model for Individual Actuator

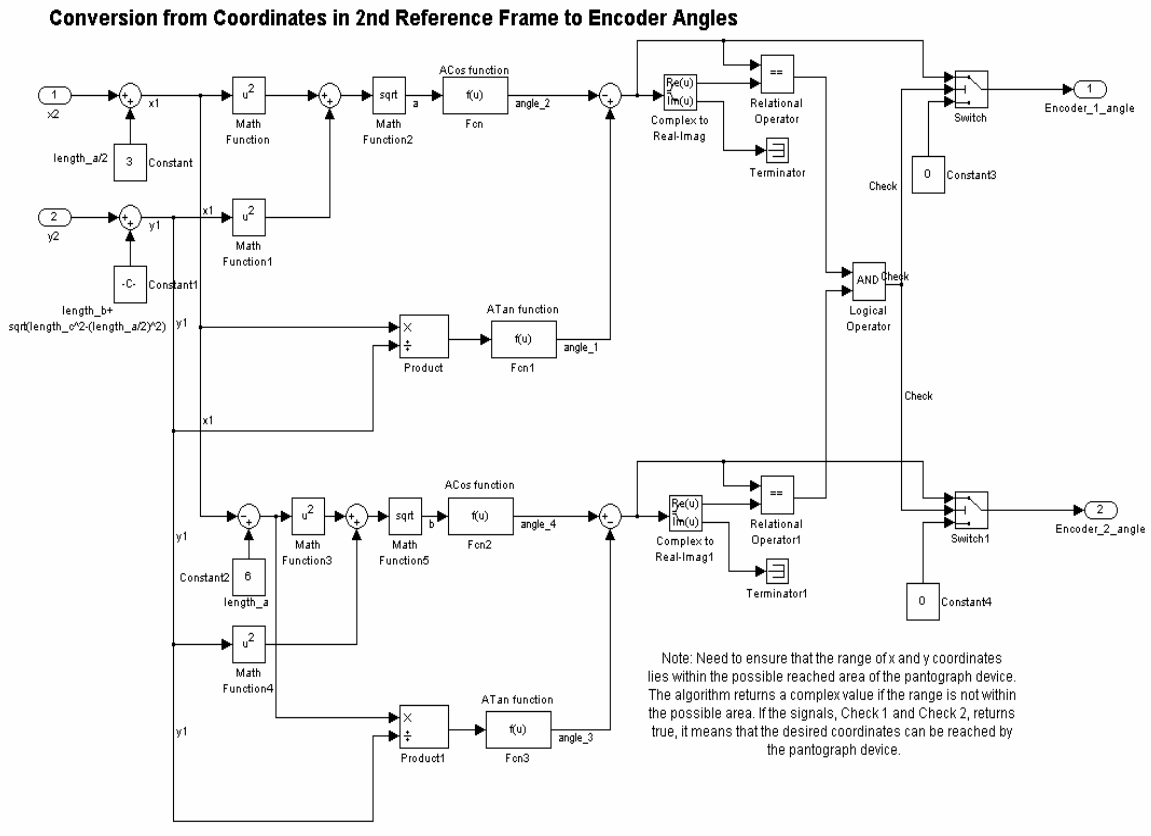

Figure C.11 Coordinate-to-Encoder-Angle Conversion Module for Pantograph Control

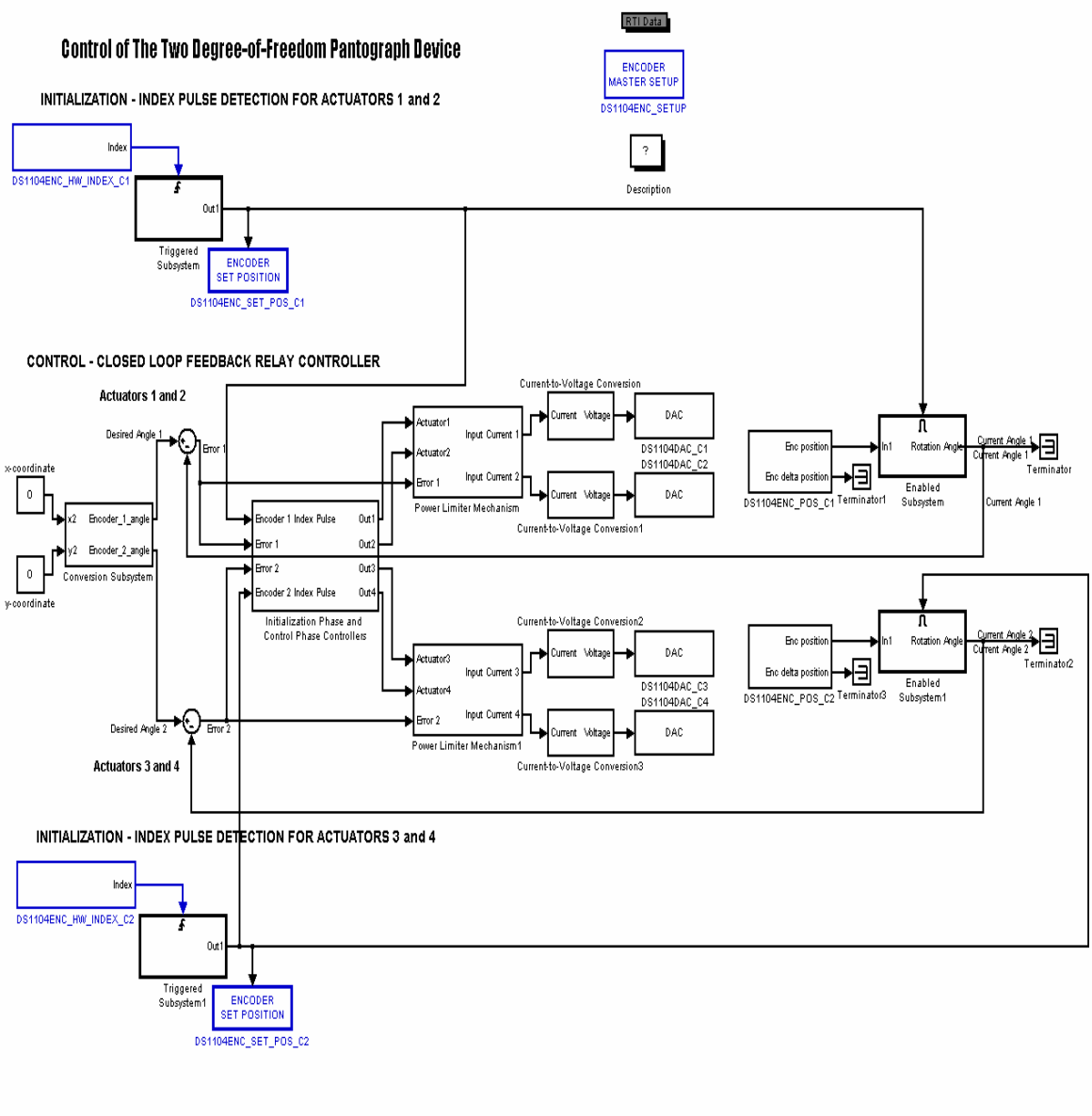

Figure C.11 Two Degree-of-Freedom Pantograph Closed Loop Control System